FORCED CONVECTION IN NANOFLUIDS OVER A FLAT PLATE

A Thesis Presented to the Faculty of the Graduate School
University of Missouri

In Partial Fulfillment
Of the Requirements for the Degree

Master of Science

by

EMILY PFAUTSCH

Dr. D.Y. Tzou, Thesis Supervisor

AUGUST 2008

The undersigned, appointed by the Dean of the Dean of the Graduate School, have examined the thesis entitles

FORCED CONVECTION IN NANOFLUIDS OVER A FLAT PLATE

Presented by Emily Pfautsch

A candidate for the degree of Masters of Science

And hereby certify that in their opinion it is worthy of acceptance.

_____

Professor D.Y. Tzou

_____

Professor Yuwen Zhang

_____

Professor John Viator

ACKNOWLEDGEMENTS

I would like to thank Dr. Tzou for being such a wonderful mentor and motivator to me throughout my undergraduate and graduate education. I would also like to thank my parents for supporting me through my education and for being such good role models.

TABLE OF CONTENTS

LIST OF FIGURES

NOMENCLATURE

δ	boundary layer thickness
ϕ	volume fraction of nanoparticles in nanofluid
λ	mean free path
μ	viscosity
ρ	density
τ	stress tensor
c	specific Heat
d	diameter
D	diffusion coefficient
h	internal energy
j	mass flux
k	thermal conductivity
k_B	Boltzmann's constant
Kn	Knudsen number
L	length of wire
$\dot{M}$	mass generation rate
S	surface
T	temperature
t	time
u	velocity in the x direction
v	velocity in the y direction
V	volume
Ve	velocity
Q	internal heat generation, power

Subscripts

bf	bulk fluid property
B	brownian motion
p	nanoparticle property
T	thermophoresis

ABSTRACT

This work analyzes the characteristics, flow development, and heat transfer coefficient of nanofluids under laminar forced convection over a flat plate. Nanofluids are engineered colloids composed of a base fluid and nanometer sized particles. They are studied because they have been shown to possess enhanced heat transfer properties over those of the base fluid. This analysis studies alumina nanoparticles submersed in water and also alumina nanoparticles submersed in ethylene glycol. A system of equations for continuity, momentum, and energy was developed and solved using Mathematica.

Nanoparticle diameter size, nanoparticle volume fraction, nanofluid temperature, and free stream velocity were varied to observe their effects on nanofluid characteristics and the heat transfer coefficient. The nanoparticle volume fraction and nanoparticle size proved to be the most dominate parameters of those that were studied. Ethylene glycol showed greater enhancements due to adding nanoparticles than did water, which corroborates with the results from other research.

The transition to a fully developed velocity profile was observed for both types of nanofluids. Despite the fact that the density/viscosity ratio of ethylene glycol is an order of magnitude smaller than water, the velocity profile became fully developed in a shorter distance along the plate than did water. In addition, increasing the free stream velocity for both types of nanofluid caused the velocity profile to develop a farther distance down the plate.

Varying the nanoparticle volume fraction distribution showed that it is vital for the nanoparticles to stay evenly suspended throughout the fluid for there to be any enhancement in the heat transfer coefficient. When the nanoparticles were evenly distributed, the heat transfer coefficient increased anywhere from 2 to 3 times compared to nanofluids with settled nanoparticles.

As the nanoparticle size was decreased below a nanometer, there was a significant increase in the heat transfer coefficient, about a 16% increase in the heat transfer coefficient for the water based nanofluid and about a 100% increase for the ethylene glycol based nanofluid. Decreasing the nanoparticle size also dispersed the volume fraction of the nanoparticles farther away from the plate and lowered the temperature next to the plate.

1. INTRODUCTION

Nanofluids are engineered colloids made of a base fluid and nanoparticles. Nanoparticles are particles that are between 1 and 100 nm in diameter. Nanofluids typically employ metal or metal oxide nanoparticles, such as copper and alumina, and the base fluid is usually a conductive fluid, such as water or ethylene glycol. Nanofluids commonly contain up to a 5% volume fraction of nanoparticles to see effective heat transfer enhancements. Nanofluids are studied because of their heat transfer properties: they enhance the thermal conductivity and convective properties over the properties of the base fluid. Typical thermal conductivity enhancements are in the range of 15-40% over the base fluid and heat transfer coefficient enhancements have been found up to 40% [1]. Increases in thermal conductivity of this magnitude cannot be solely attributed to the higher thermal conductivity of the added nanoparticles, and there must be other mechanisms attributed to the increase in performance.

Fluid heating and cooling are important in many industries such as power, manufacturing, transportation, and electronics. Effective cooling techniques are greatly needed for cooling any sort of high-energy device. Common heat transfer fluids such as water, ethylene glycol, and engine oil have limited heat transfer capabilities due to their low heat transfer properties. In contrast, metals have thermal conductivities up to three times higher than these fluids, so it is natural that it would be desired to combine the two substances to produce a heat transfer medium that behaves like a fluid, but has the thermal conductivity of a metal.

Prior to the development of production methods for creating nano-sized particles of metals and metal oxides, some research was done on the effects of putting millimeter or micrometer sized particles inside fluid. Although these particles helped improve the thermal conductivity of the fluid, they created other problems in terms of settling, producing drastic pressure drops, clogging channels, and premature wear on channels and components. Nano-sized particles have an advantage over even micro-sized particles because they approach the size of the molecules in the fluid, which helps prevent the nanoparticles from settling due to gravity and causing clogging and wearing. Figure 1 shows the size of nanoparticles inside of ethylene glycol.

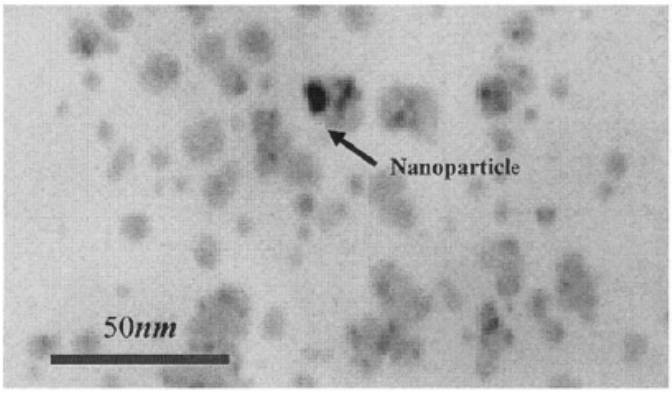

Fig. 1. Bright-field transmission electron micrograph of copper nanoparticles (< 10nm) in ethylene glycol [2].

The idea of putting small metal particles in fluid to enhance the fluid's heat transfer properties is nothing new, as it was documented by Maxwell in 1904 [3]. Fluid thermal conductivity models have been proposed by Maxwell [3] and Hamilton and Crosser [4], which are effective for calculating thermal conductivities of fluids with micro or larger sized particles [5], but neither can

predict the enhanced thermal conductivities of the nanofluids because the models do not include any dependence on particle size [6].

1.1 Production of Nanoparticles and Nanofluid

Nanoparticles are made in one of two ways: physical processes and chemical processes. The physical techniques include mechanical grinding and the inert gas condensation technique. The chemical processes include chemical precipitation, spray pyrolysis, and thermal spraying.

There are also two ways to produce nanofluids, by a one-step process or a two-step process. The one-step process simultaneously makes and disperses the nanoparticles directly into the base fluid, while with the two-step process, the nanoparticles are made and then dispersed in the fluid. The major disadvantage of the two step process is that the nanoparticles tend to agglomerate before the nanoparticles can be dispersed in the fluid. The one-step process is also favorable because it prevents oxidation of the nanoparticles [1].

1.2 Heat Transfer Variables in Nanofluids

The heat transfer enhancement in nanofluids has been attributed to many mechanisms, and each will be discussed individually. As the reader will see, most research has been done on how variables affect the effective thermal conductivity, not the heat transfer coefficient independently.

1) *Particle Agglomeration*

One challenge with nanofluids is that the nanoparticles tend to agglomerate due to molecular forces such as Van Der Waals force [7, 8]. Karthikeyan, Philip, and Raj [7] found in their experiments with copper oxide/water nanofluid that the nanoparticle size and cluster size have a significant influence on thermal conductivity. They also found that agglomeration is time-dependent. As time elapsed in their experiment, agglomeration increased, which decreased the thermal conductivity. Figure 2 shows how the thermal conductivity decreases with time.

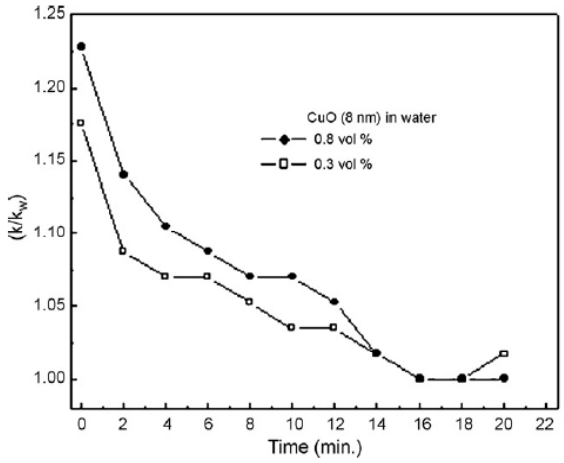

Fig. 2. Time dependence of thermal conductivity for copper oxide/water nanofluid [7].

From Fig. 2, it can be seen that the thermal conductivity of the nanofluid drops dramatically as time increases, which Karthikeyan, Philip, and Raj attribute to particle agglomeration. They confirmed this theory microscopically, which is shown in Fig. 3.

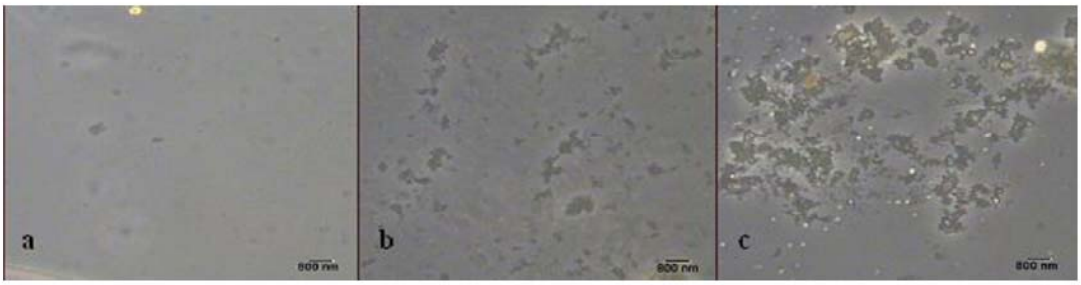

Fig. 3. 0.1% volume fraction of copper oxide nanoparticles in water after a) 20 minutes b) 60 minutes c) 70 minutes [7].

As one can see in the figure, the clustering of the nanoparticles greatly increases with time, and it is noticeable after only 60 minutes. Karthikeyan, Philip, and Raj observed that there was no sedimentation when the photos were taken. Agglomeration causes the effective surface area to volume ratio of the nanoparticles to decrease, which reduces the thermal conductivity of the fluid. The group also concluded that agglomeration increases with increasing nanoparticle concentration because the particles are closer together and experience more Van Der Waals attraction. Wang [9] measured the viscosity of alumina-water nanofluid and found that viscosity increases as nanoparticles agglomerate, which could also contribute to the lower thermal conductivity when agglomeration increases.

2) *Volume Fraction*

Effective thermal conductivity of nanofluid increases with increasing volume fraction of nanoparticles [7], but as the volume fraction of nanoparticles increases, it may no longer be valid to assume that the

nanoparticles stay suspended. This is why it is more effective to use a very small volume fraction in nanofluids [2].

3) Brownian Motion

Several researchers have found that Brownian motion, which is the random movement of particles, is one of the key heat transfer mechanisms in nanofluids [10, 11]. It is thought to cause a microconvection effect. Brownian motion only exists when the particles in the fluid are extremely small, and as the size of the particles gets larger, Brownian motion effects diminish [12].

4) Thermophoresis

Thermophoresis occurs because of kinetic theory in which high energy molecules in a warmer region of liquid impinge on the molecules with greater momentum than molecules from a cold region. This leads to a migration of particles in the direction opposite the temperature gradient, from warmer areas to cooler areas.

5) Nanoparticle size

Several studies have found that as nanoparticles are reduced in size, the effective thermal conductivity of the nanofluid increases [11]. This is because of two reasons. As the nanoparticle size is reduced, Brownian motion is induced. Also, lighter and smaller nanoparticles are better at

resisting sedimentation, one of the biggest technical challenges in experimenting with nanofluids [12].

6) Particle shape/surface area

Several studies have found that rod-shaped nanoparticles, such as carbon nanotubes, remove more heat than spherical nanoparticles [1, 13, 14,15]. This may be due to the fact that rod-shaped particles have a larger aspect ratio (the ratio between a particle's surface area to volume) than spherical nanoparticles.

7) Liquid layering on the nanoparticle-liquid interface

Some researchers have suggested that there is liquid layering on the nanoparticles, which helps enhance the heat transfer properties of the nanofluid. The thickness and thermal conductivity of the nanolayer are not known yet, but the liquid molecules close to a solid surface have been proven by Yu, Richter, Datta, et. al. [16] to form layers. Ren, Xie, and Cai [5] made a theoretical model to study the change in thermal conductivity from adding liquid layering on the nanoparticles. They assumed that the thermal conductivity of the layer would be somewhere between the thermal conductivity of the bulk fluid and the nanoparticle. They found that an increase in the layer thickness leads to a large thermal conductivity enhancement. Their results are shown in Fig. 4.

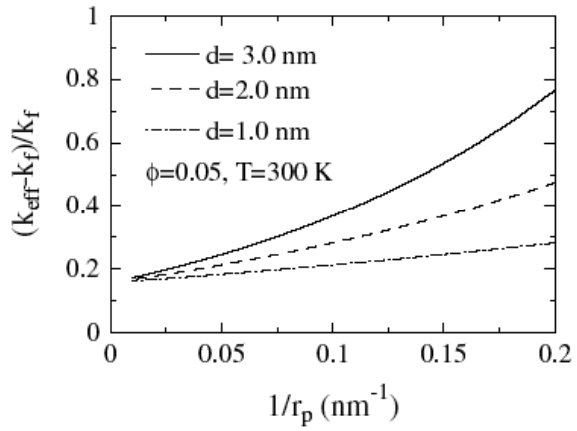

Fig. 4. Dependence of thermal conductivity enhancement on the reciprocal of the nanoparticle radius [5].

In the figure, d is the thickness of the liquid layering, and r_p is the nanoparticle radius. As one can see, the thermal conductivity of the nanofluid goes up with increasing surface layering. Ren, Xie, and Cai also found that as the nanoparticles increased in size, the effects of the liquid layering became weaker.

8) Temperature

Nanofluids' effective thermal conductivity and Brownian motion increase with temperature [2, 11, 17, 12]. Chon, Kihm, Lee and Choi [11] did an experimental investigation of alumina nanofluids and how their thermal conductivity varies with temperature. Figure 5 shows their results.

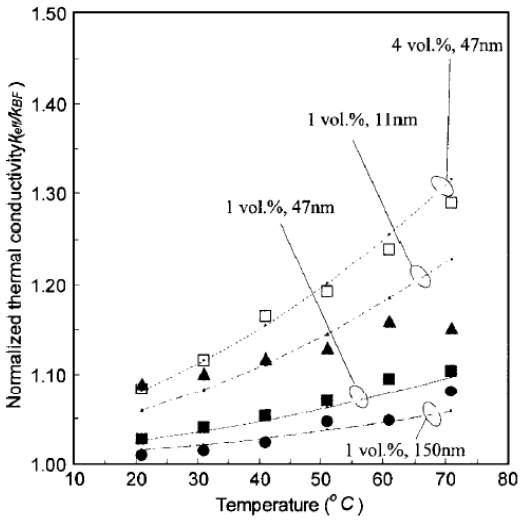

Fig. 5. Experimental results of thermal conductivity dependence on temperature [11].

From Fig. 5, it is evident that the normalized thermal conductivity, or the ratio of the thermal conductivity of the nanofluid to the thermal conductivity of the base fluid, is highly dependent upon temperature as well as volume fraction of nanoparticles. As the temperature and volume fraction of nanparticles increase, the thermal conductivity increases as well.

9) *Reduction in thermal boundary layer thickness.*

Several researchers have mentioned that a reduction in the thermal boundary layer thickness may be a mechanism that causes heat transfer enhancements in nanofluids, but there has been very little research in the area to date.

Research with nanofluids is still fairly new, so some of the mechanisms that affect heat transport in nanofluid have yet to be studied in depth. In addition, most

research has been done on mechanisms that affect thermal conductivity and not as much research has been done on mechanisms that affect the heat transfer coefficient in convection. More research is needed in all of the areas listed in section 1.2 before heat transfer mechanisms can be well understood.

1.3 Establishing Nanofluid Properties

1.3.1 Thermal Conductivity

The majority of nanofluid research has been on establishing the thermal conductivity of nanofluids [15], which was discussed more extensively in section 1.2 on heat transfer variables of nanofluids. Some researchers have found moderate enhancements in thermal conductivity, but many have observed large enhancements. For instance, Garg, Poudel, Chiesa, et. al. [18] found from testing copper/ethylene glycol nanofluid, that the thermal conductivity was twice the amount as what is predicted by the Maxwell effective medium theory.

1.3.1.1 Measuring Thermal Conductivity

The most common way of measuring thermal conductivity in nanofluids is by the transient hot wire method. A thin platinum wire is coated with an electrically insulating layer. The wire is immersed in the nanofluid and a constant current is passed through it. The temperature rise of the wire is measured as a function of time. The thermal conductivity can be measured using Eq. (1).

$$k = \frac{Q}{4\pi L \frac{dT}{d\ln t}} \qquad \text{Eq. (1)}$$

where k is the thermal conductivity of the nanofluid, Q is the total power dissipated in the wire, L is the length of the wire, T is the wire temperature, and t is the time. In order to measure the temperature rise, the hot wire is made part of a Wheatstone bridge. The change in the wire temperature causes a change in the wire resistance, which causes the bridge to become imbalanced. The change in the wire resistance is calculated from the voltage imbalance in the bridge. The change in wire resistance is compared to data that correlates the change in wire resistance to a change in temperature, and the temperature difference is obtained [18]. Using the transient hot wire technique correlates a coefficient to the temperature drop, and it should be pointed out that this coefficient encompasses all forms of heat transfer that may be taking place, whether it is conduction, nanoconvection, or any other mode of heat transfer.

1.3.2 Heat Capacity

The heat capacity of the nanofluid is incorporated into the energy equation, so it is important to be able to calculate it accurately. Most researchers use one of two correlations, which are in Eq. (2),

$$c = (1-\phi)c_{bf} + \phi c_p \qquad \text{Eq. (2a)}$$

$$c = \frac{(1-\phi)(\rho c)_{bf} + \phi(\rho c)_p}{\rho} \qquad \text{Eq. (2b)}$$

where c is the heat capacity, ϕ is the volume fraction of nanoparticles, and ρ is density. The subscript *bf* refers to properties of the base fluid and the subscript p refers to properties of the nanoparticles. Equation (2a) is simply the rule of mixtures applied to heat capacity, while Eq. (2b) is an altered form. Mansour,

Galanis, and Nguyen [19] plotted both functions as a ratio to the specific heat of the base fluid with respect to the nanoparticle concentration in the nanofluid. Their results for alumina nanoparticles and water are shown in Fig. 6.

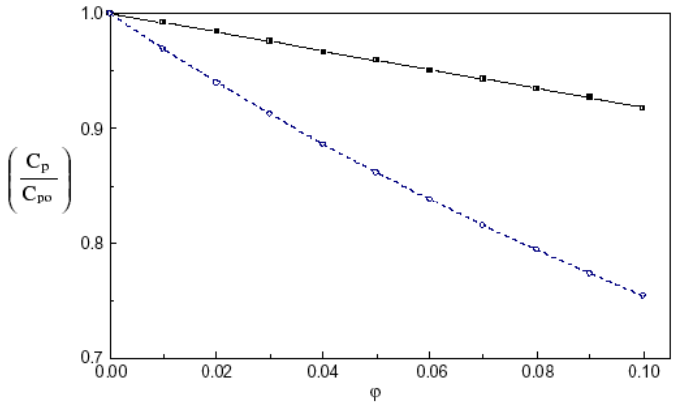

Fig. 6. Comparison of heat capacity formulas (blue open circles: Eq. (2a), black solid circles: (2b)) [19].

From Fig. (6), it can be seen that Eq. (2a) is much lower than Eq. (2b). Mansour, Glanis, and Nguyen were not sure which correlation was correct, so they assumed both to be valid, but Zhou and Ni [20] investigated both correlations more closely, and found that Eq. (2b) is valid. Their results for alumina nanoparticles in water, which mimic those of Mansour, Glanis, and Nguyen, are shown in Fig. 7.

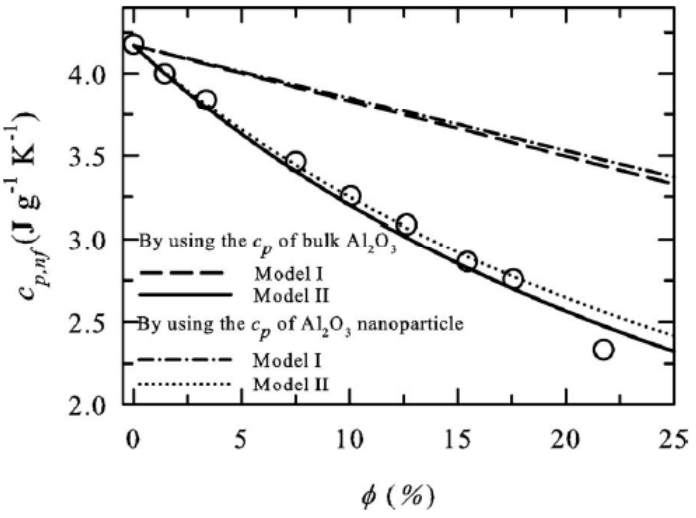

Fig. 7. Comparison of specific heat correlations for Eq. (2a) and Eq. (2b), which correspond to Model I and Model II in the figure, respectively. Open circles are experimental data that is being compared to the two correlations [20].

In Fig. 7, Model I of the figure is Eq. (2a) and Model II is Eq. (2b). The circles are the experimental data obtained by Zhou and Ni, and they collapse very well onto Eq. (2b), proving that Eq. (2b) is the best specific heat correlation to use in predicting behavior in nanofluids.

1.3.3 Viscosity

Prasher, Song, Wang, et al. [21] published a paper solely on the experimental results of the viscosity of alumina particles in propylene glycol, and its dependency on particle diameter, nanoparticle volume fraction, and temperature. They found that the viscosity of nanofluids is extremely dependent on nanoparticle volume fraction, but is independent of the shear rate, nanoparticle diameter, and temperature. The fact that the nanofluid viscosity is independent of shear rate and nanoparticle diameter indicates that the nanofluid

obeys Newtonian behavior. Figure 8 shows the dependence of viscosity on the nanoparticle volume fraction.

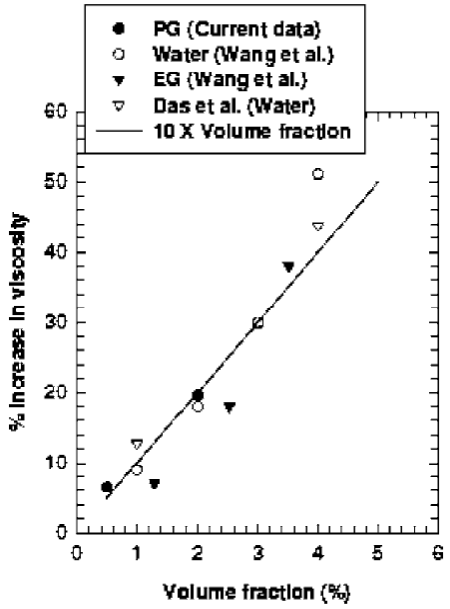

Fig. 8. Nanofluid viscosity dependence on volume fraction [21].

In Fig. 8, the percent increase in viscosity on the y axis is comparing the viscosity of the nanofluid to the viscosity of the base fluid. As can be seen, the viscosity is highly dependent on the volume fraction of nanoparticles and Prasher, Song, Wang et. al. suggest that nanofluids follow the Einstein law of viscosity for low nanoparticle volume fractions, but not for large volume fractions because the nanoparticles start to aggregate in the nanofluid. Figure 8 includes data from other researchers as well. From this data, it is possible for the increase in viscosity can be larger than the increase in thermal conductivity.

Garg, Poudel, Chiesa, et. al. [18] conducted an experiment to test the viscosity of copper nanoparticles in ethylene glycol and found that the increase in

viscosity was about four times of that predicted by the Einstein law of viscosity, which is given in Eq. (3),

$$\frac{\mu}{\mu_{bf}} = 1 + 2.5\phi, \qquad \text{Eq. (3)}$$

where μ is the viscosity of the nanofluid, μ_{bf} is the viscosity of the base fluid, and ϕ is the nanoparticle volume fraction. Figure 9 shows the results of their study.

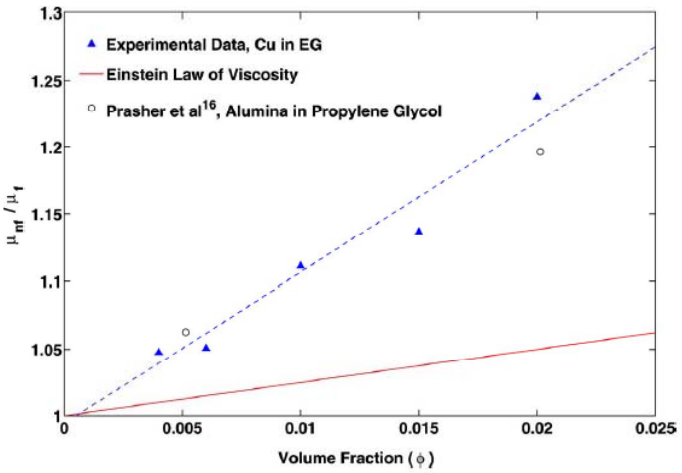

Fig. 9. Viscosity of copper in ethylene glycol nanofluid [18].

As can be seen from Fig. 9, the Einstein law of viscosity drastically underestimates the experimental results. Garg, Poudel, Chiesa, et. al. found that the 2.5 in Eq. (3) should be about 11 to correlate with their data. They also noted that with such a high viscosity, flow in very small tubes would not be effective in heat transfer, and that larger tubes would be more effective.

In Pak and Cho's [22] experimental study of turbulence of alumina/water and titanium oxide/water nanofluid in a round pipe, they found that viscosity increased 200 times that of water for water with 10% volume fraction of alumina

and they found a 3 times increase for 10% volume fraction of titanium oxide nanoparticles in water. Their results are shown in Fig. 10.

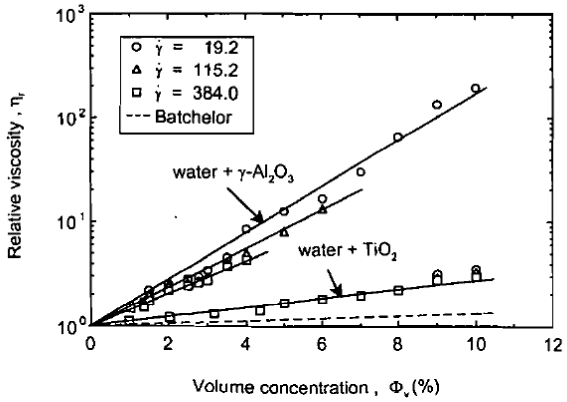

Fig. 10. Relative viscosity versus volume concentration of nanoparticles at different shear rates [22].

Once again, the relative viscosity is the ratio of the viscosity of the nanofluid to the viscosity of the base fluid. Pak and Cho also found that the viscosity decreases with increasing temperature, which is shown by Fig. 11.

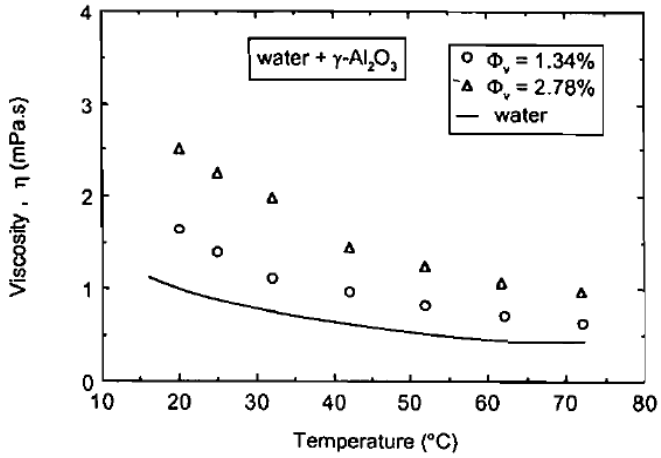

Fig. 11. Temperature effects of viscosity of nanofluids with alumina nanoparticles (13 nm diameter) [22].

Pak and Cho observed that the viscosities of the nanofluids decreased asymptotically with increasing temperature, and the rate of decrease of the

viscosity became greater as the volume fraction increased. Pak and Cho suggest that the increase in viscosity may be due to the viscoelectric effect, which is due to the fact that the effective particle dimension is larger than its radius and equal to the Debye length (the scale over which electrons screen out electric fields). Pak and Cho also found that the sphere size and shape has an effect on viscosity. As the sphere diameter is decreased and the sphere shape becomes more irregular, the viscosity increases. The irregular shape of the nanoparticle is thought to increase viscosity because the surface area to volume ratio is increased.

2. Review of Nanofluid Convection Literature

To date, there has been little research involving convection, especially forced convection [23]. Most research has been focused on determining the thermal conductivity of nanofluids and not much attention has been given to finding the heat transfer coefficient from convection. Of the research that is available for forced convection, most researchers have analyzed forced convection of nanofluids in a tube [22, 23, 24, 25, 26], not over a flat plate, as this analysis does. There has been some nanofluid forced convection research over a flat plate, but it is with application to pool boiling for use in nuclear reactors. The following sections cover the research that has been done with convection, especially forced convection, thus far.

2.1 Heat Transfer Enhancement by Using Nanofluids in Forced Convection Flows [24]

S. E. B. Maiga, S. J. Palm, C. T. Nguyen, G. Roy, N. Galanis

Maiga, Palm, Nguyen et. al. [24] studied laminar forced convection in a uniformly heated tube, using a CFD code. They used alumina particles suspended in water and also in ethylene glycol. They found that the heat transfer coefficient and the wall shear stress increase with increasing nanoparticle volume fraction and Reynolds number. Maiga, Palm, Nguyen et. al. also found that the heat transfer enhancement was more pronounced in the ethylene glycol mixture than

in the water mixture. The ethylene glycol produced more adverse effects on the wall shear stress. In their study, φ is the volume concentration of nanoparticles, R is the radial position inside the tube, D is the diameter of the tube, R_o is the radius of the tube, Z is the length along the tube, T is the temperature of the nanofluid, h_r is the ratio of the heat transfer coefficient of the nanofluid to the heat transfer coefficient of the base fluid, and τ_r is the ratio of the wall shear stress of the nanofluid to the wall shear stress of the base fluid. All of the results presented are for a water/alumina mixture with a Reynolds number of 500 and a wall heat flux of 10,000 W/m^2, but the same behaviors were found in the ethylene glycol mixture. Figure 12 shows the effect of particle volume fraction on the radial temperature profile.

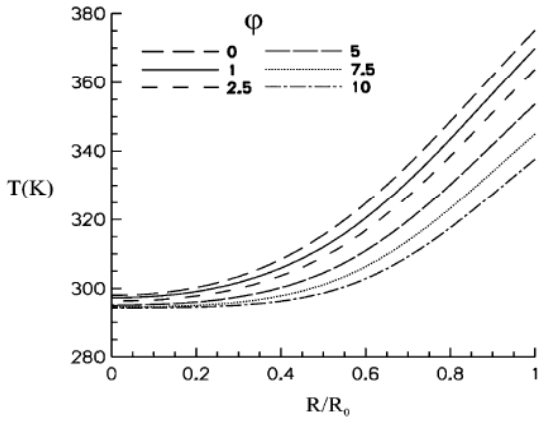

Fig. 12. Effect of parameter φ on fluid temperature profiles [24].

As can be seen from Fig. 12, the fluid temperatures decrease with an increase of φ, especially near the tube wall where $R/R_o=0$, indicating that there is a higher heat transfer rate with the nanoparticles. Maiga, Palm, Nguyen et. al. found in Fig. 13 that the wall temperature of the pipe varies more with nanoparticle

volume fraction than the temperature of the base fluid, proving that more heat is being removed next the wall of the tube.

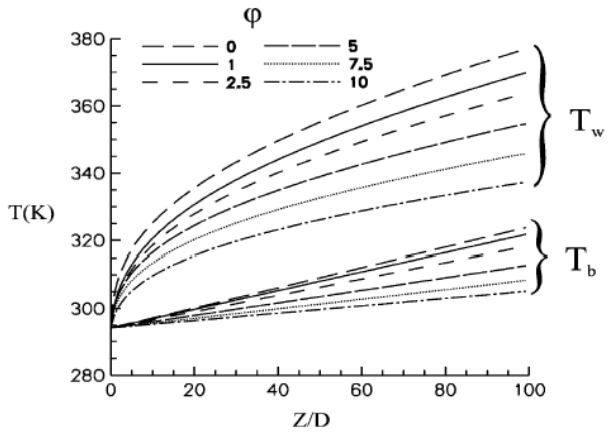

Fig. 13. Effect of φ on axial development of fluid bulk and wall temperature [24].

It can also be observed that the decrease in fluid temperature does not take place along the entire length of the tube, and the largest decrease occurs at the tube exit. From Fig. 12-13, there is an obvious heat transfer enhancement due to adding nanoparticles to the fluid. Figure 14 plots the heat transfer coefficient with respect to the tube length.

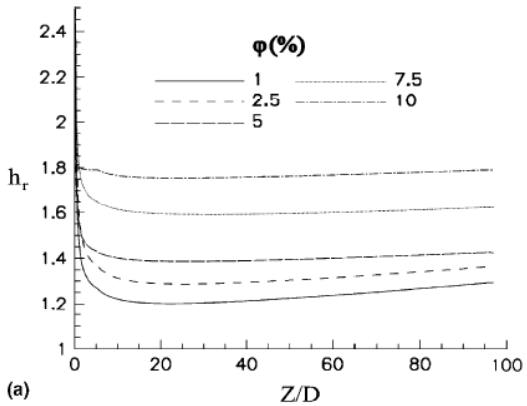

Fig. 14. Effect of φ on heat transfer coefficient ratio h_T [24].

As can be seen from Fig. 14, the heat transfer coefficient increases are very significant, being as much as 63% higher than the heat transfer coefficient of the base fluid. The heat transfer ratio clearly increases as nanoparticle volume fraction increases. Towards the end of the tube length, the heat transfer ratio appears to level off, except for the lower nanoparticle volume fractions, which are slightly increasing toward the tube end. Figure 15 shows the effect that the nanoparticle volume fraction has on the wall shear stress.

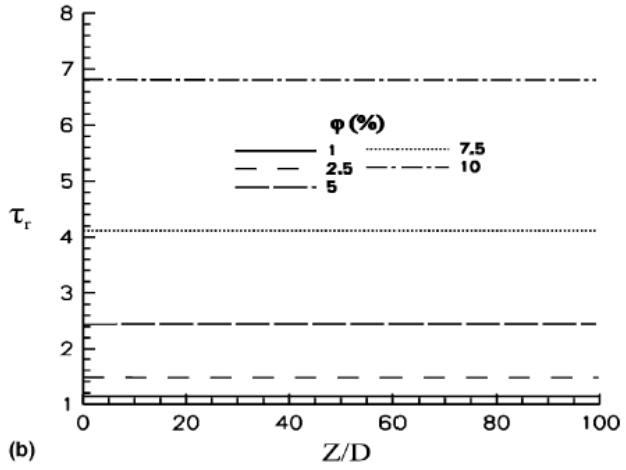

Fig. 15. Effect of φ on wall shear stress ration τ_r [24].

One can observe that the wall shear stress ratio remains constant along the tube length and greatly increases with nanoparticle volume fraction, with the shear stress more than quadrupling in the case of φ=7.5%.

Maiga, Palm, Nguyen et. al. found that for laminar forced convection inside a tube, the heat transfer coefficient and wall shear stress both increase with increasing nanoparticle volume fraction. Ethylene glycol was found to remove the most heat, but also had the highest increase in wall shear stress.

However, their study did not include an optimum nanoparticle volume fraction for heat transfer. Most likely, there is a point where adding more nanoparticles to the nanofluid becomes counterproductive in removing heat due to agglomeration.

2.2 Experimental Investigation of Convective Heat Transfer of Al_2O_3/water Nanofluid in a Circular Tube [25]

S. Z. Heris, M. N. Esfahany, S. G. Etemad

Heris, Esfahany, and Etemad [25] completed a similar study to Maiga, Palm, Nguyen, et. al except that it includes experimental results as opposed to numerial results. They analyzed laminar forced convection of alumina/water nanofluid inside a circular tube with a constant wall temperature. They too found that the heat transfer coefficient increases by increasing the concentration of nanoparticles in nanofluid. Heris, Esfahany, and Etemad plotted all of their results against the Peclet number, which relates the rate of advection to the rate of diffusion, and is given in Eq. (4),

$$Pe = \mathrm{Re}\,\mathrm{Pr} = \frac{\overline{U}D}{\alpha}, \qquad \text{Eq. (4)}$$

where *Pe* is the Peclet number, *Re* is the Reynolds number, *Pr* is the Prandtl number, $\overline{U}$ is the free stream velocity, *D* is the Diameter of the tube, and α is the thermal diffusivity. Figure 16 shows the heat transfer coefficient of the nanofluid versus the Peclet number, and also compares it against theoretical results.

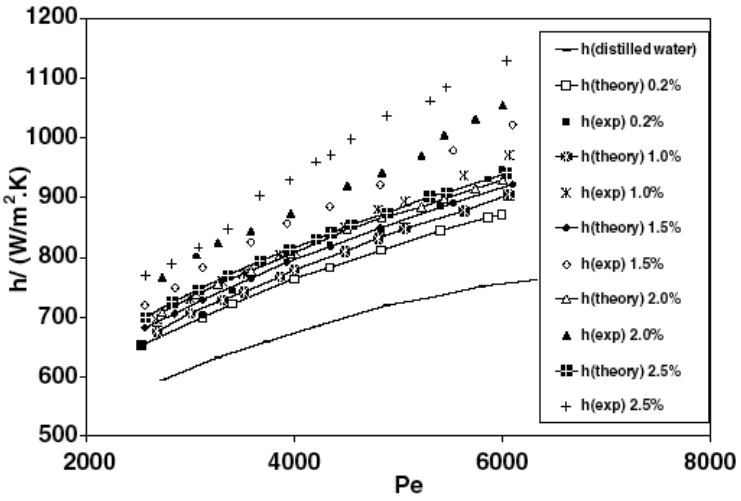

Fig. 16. Experimental values of the heat transfer coefficient and calculated values from Seider-Tate equation for alumina/water nanofluid versus Peclet number at different volume concentrations [25].

The theoretical results that are being compared to the experimental results in Fig. 16 come from the Seider-Tate correlation, which only takes into account an increase in thermal conductivity as a mode of heat transfer enhancement. As can be seen from Fig. 16, all of the heat transfer coefficients from the experimental results of nanofluids are higher than the theoretical results. In addition, the experimental results are all much higher than the heat transfer coefficient of water without nanoparticles. Since the Seider-Tate equation only accounts for an increase in thermal conductivity, which has a heat transfer coefficient that is routinely lower than the experimental heat transfer coefficient, it is obvious from Fig. 16 that there are more mechanisms that are producing the heat transfer enhancement, such as nanoparticle clustering, nanoconvection, and other dynamic conditions.

2.3 *Prediction of Turbulent Forced Convection of a Nanofluid in a Tube with Uniform Heat Flux using a Two Phase Approach [23]*

A. Behzadmeh, M. Saffar-Avval, N. Galanis

Behzadmehr, Saffar-Avval, and Galanis investigated turbulent forced convection heat transfer in a circular tube with 1% volume fraction copper nanoparticles in water. They did this using a numerical model of a two-phase approach, meaning that the nanoparticles are not assumed to have the same velocity as the fluid. In this study, Z is the tube length, D is the tube diameter, k_c is the turbulent kinetic energy, and Nu is the Nusselt number. Figure 17 shows the turbulent kinetic energy at the tube centerline with respect to the tube length.

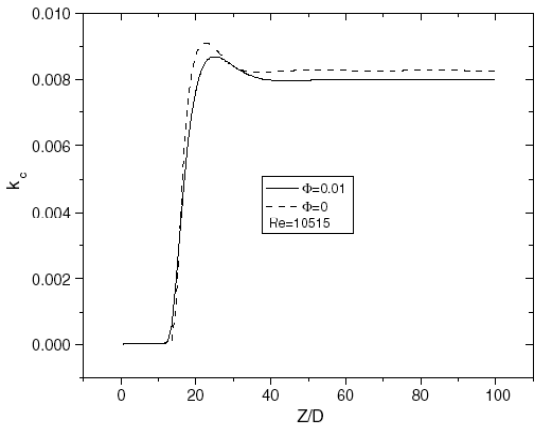

Fig. 17. Axial evolution of the centerline turbulent kinetic energy for pure water and nanofluid [23].

The results from Fig. 17 indicate that the turbulence becomes fully developed at Z/D=50. The rapid increase in kinetic energy corresponds to the point where the diffusing turbulence reaches the tube centerline. From Fig. 17, the nanofluid

exhibits lower values of turbulent kinetic energy than the water, which means that the nanoparticles are absorbing some of the energy of the velocity and fluctuations. This trend is true for higher particle concentrations, and as particle concentrations increase, the turbulent kinetic energy decreases. Behzadmehr, Saffar-Avval, and Galanis also plotted the Nusselt number versus the length of the tube, which is shown in Fig. 18.

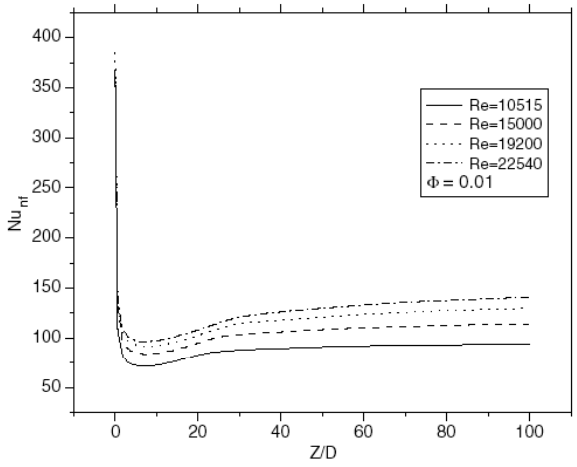

Fig. 18. Nusselt number along the tube axis [23].

From Fig. 18, it can be observed that the increasing Reynolds number causes the Nusselt number and the heat transfer coefficient to increase.

In summary, Behzadmehr, Saffar-Avval, and Galanis found that adding nanoparticles in turbulent forced convection is effective in enhancing the heat transfer capabilities of the base fluid. The nanoparticles can absorb the velocity fluctuation energy to reduce the turbulent kinetic energy.

2.4 Hydrodynamic and Heat Transfer Study of Dispersed Fluids with Submicron Metallic Oxide Particles [22]

B. C. Pak, Y. I. Cho

Pak and Cho conducted experimental investigations on turbulent friction and heat transfer of nanofluids in a circular pipe. They tested alumina and titanium oxide nanoparticles with mean diameters of 13 and 27 nm, respectively, in water. They found that putting a 10% volume fraction of alumina in water increased the viscosity of the fluid 200 times and putting the same volume fraction of titanium oxide produced a viscosity that was 3 times greater than water. They also found that the nanofluids friction factor corresponded well with the Kays correlation for turbulent flow, as have other researchers. They compared the heat transfer coefficient against the Reynolds number, and their results are shown in Fig. 19.

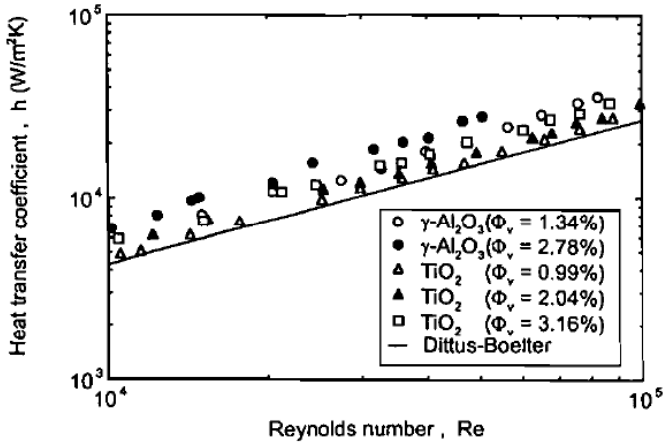

Fig. 19. Heat transfer coefficient versus Reynolds number for titanium oxide/water and alumina/water nanofluids [22].

From Fig. 19, the heat transfer coefficient increased 45% at 1.34% volume fraction of alumina to 75% at 2.78% volume fraction of alumina. The alumina nanofluid is consistently higher than the titanium oxide nanofluid. Pak and Cho attributed this effect to “enhanced mixing caused by submicron particles near the walls” [22]. They plotted the Nusselt number versus the Reynolds number, and the Nusselt number followed the same trend as the heat transfer coefficient in Fig. 19.

2.5 Investigation on Convective Heat Transfer and Flow Features of Nanofluids [26]

Y. Xuan and Q. Li

Xuan and Li conducted an experimental investigation on turbulent convective heat transfer of nanofluids in a tube. They took into account volume fraction and Reynolds number. Copper nanoparticles below 100 nm in diameter were mixed with deionized water, and the nanoparticle concentration varied from 0.3% to 2.0% percent. The heat transfer coefficient calculated from their experiment is shown in Fig. 20.

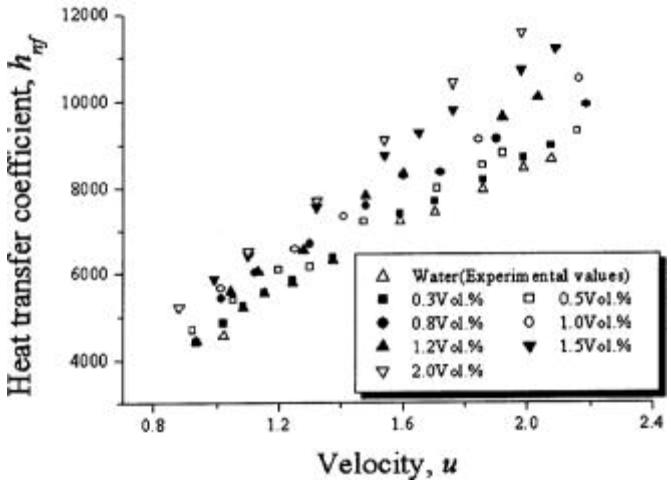

Fig. 20. Variation of heat transfer coefficient with velocity in turbulent flow [26].

As can be seen in Fig. 20, the convective heat transfer coefficient increases with the fluid velocity as well as the nanoparticle concentration. All of the nanofluids shown have an increase in the heat transfer coefficient over that of water. Xuan and Li point out that at higher nanoparticle volume fractions, the viscosity increases sharply, which suppresses heat transfer enhancement in the nanofluid. Therefore, it is important to carefully select the proper nanoparticle volume fraction to achieve heat transfer enhancement.

2.6 Convective Transport in Nanofluids [17]

J. Buongiorno

Buongiorno considered seven slip mechanisms that can produce a relative velocity between the nanoparticles and the base fluid: inertia, Brownian diffusion, thermophoresis, diffusiophoresis, Magnus effect, fluid drainage, and

gravity. Of all of these mechanisms, only Brownian diffusion and thermophoresis were found to be important. Buongiorno's analysis consisted of a two-component equilibrium model for mass, momentum, and heat transport in nanofluids. He found that a nondimensional analysis of the equations implied that energy transfer by nanoparticle dispersion is negligible, and cannot explain the abnormal heat transfer coefficient increases. Buongiorno suggests that the boundary layer has different properties because of the effect of temperature and thermophoresis. The viscosity may be decreasing in the boundary layer, which would lead to heat transfer enhancement. Taking Brownian motion and thermophoresis into account, Buongiorno developed Eq. (5) or equation 50 in his paper, for the Nusselt number,

$$Nu_{bf} = \frac{\frac{f}{8}(\mathrm{Re}_{bf} - 1000)\mathrm{Pr}_{bf}}{1 + \delta_v^{+}\sqrt{\frac{f}{8}(\mathrm{Pr}_v^{\,2/3} - 1)}}, \qquad \text{Eq. (5)}$$

Where *Nu* is the Nusselt number, *f* is the friction factor, *Pr* is the Prandtl number, Re is the Reynolds number, δ_v^{+} is the dimensionless thickness of the laminar sublayer, the subscript *v* refers to the laminar sublayer, and the subscript *bf* refers to the base fluid. Buongiorno divides the boundary layer into two layers, the laminar sublayer is closest to the wall, and a turbulent sublayer is on top of the laminar sublayer. Equation (5) was compared to data from Pak and Cho, and Xuan and Li, works which were previously discussed in this paper. The results are shown in Fig. 21.

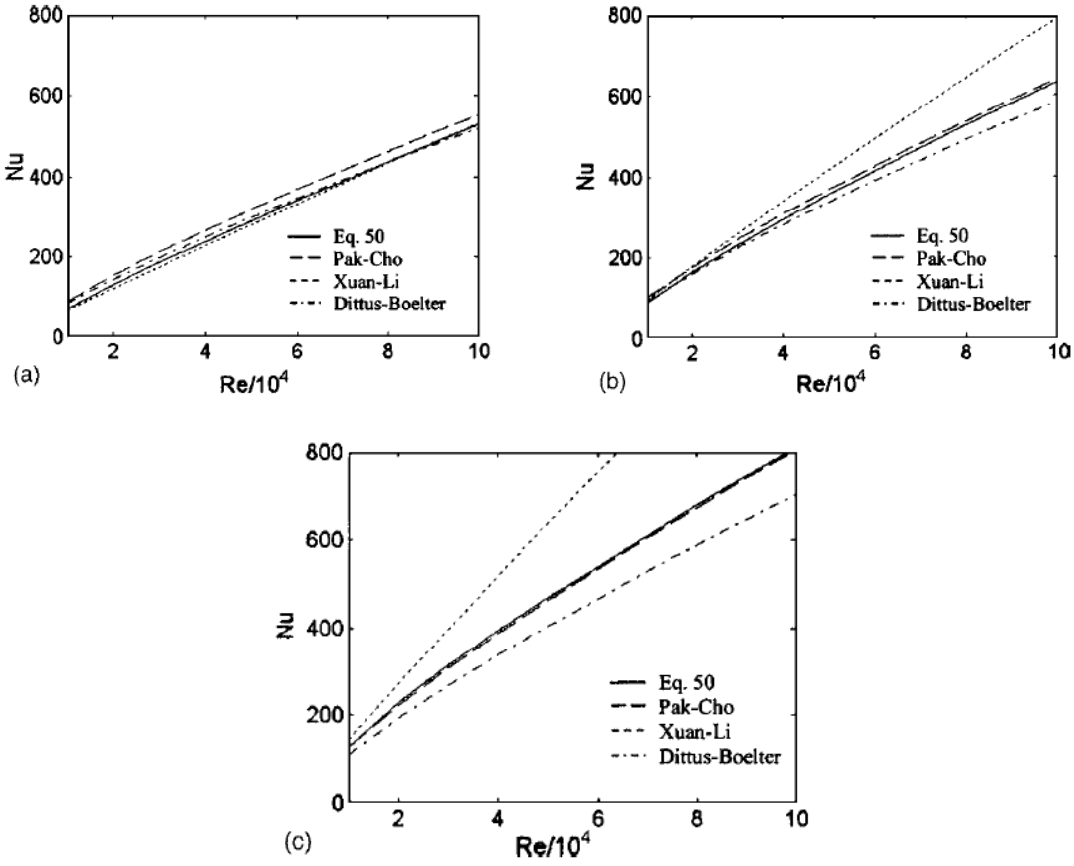

Fig. 21. Heat transfer in alumina/water nanofluids: a) $\phi = 0$ b) $\phi = 0.01$ c) $\phi = 0.03$ [17].

As one can see from the figures, the Nusselt number increases with increasing Reynolds number. Equation (5) correlates best with Pak and Cho's experimental data. As the nanoparticle volume fraction is increased, the data from all of the researchers starts to gradually diverge. Correlations for the Nusselt number do not necessarily correspond to the correlations for the heat transfer coefficient.

2.7 *Heat Transfer Enhancement using Al_2O_3-water Nanofluid for an Electronic Liquid Cooling System [27]*

C. T. Nguyen, G. Roy, C. Gauthier, N. Galanis

Nguyen, Roy, Gauthier, et. al. experimentally investigated turbulent alumina/water nanofluid for cooling microprocessors and other electric systems. They put a liquid cooling block system over a heated block and measured the heat transfer coefficient of the cooling block. They found a significant enhancement in the heat transfer coefficient from using nanofluid over the base fluid. By using 6.8% volume fraction of alumina in distilled water, the heat transfer coefficient was increased by as much as 40%. They also found that increasing the nanoparticle concentration decreased the heated component temperature. Nguyen, Roy, Gauthier, et. al. used nanoparticles of 36 nm particle diameter and 47 nm diameter, and found that the 36 nm particles produced higher heat transfer coefficients in the water block. Equation (6) shows how the heat transfer coefficient of the water block was calculated.

$$q_{electric} = h_{w-block} A(T_{m,base} - T_{m,f}) \qquad \text{Eq. (6)}$$

where $q_{electric}$ is the total electric input power, $h_{w\text{-}block}$ is the heat transfer coefficient of the cooling block, A is the total augmented surface area of the base plate, $T_{m,base}$ is the mean temperature of the base plate, and $T_{m,f}$ is the average temperature of the fluid going through the block. Figure 22 shows how $h_{w\text{-}block}$ varies with mass flow rate and nanoparticle volume fraction.

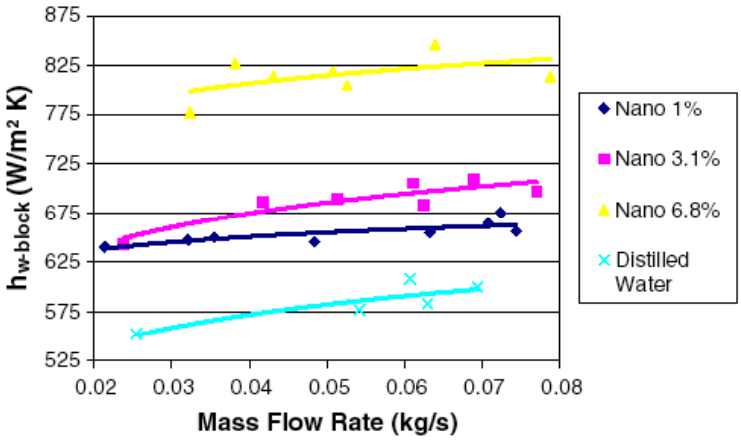

Fig. 22. Influence of mass flow rate and particle concentration on the heat transfer coefficient of the water block [27].

As can be seen from Fig. 22, the addition of nanoparticles has greatly increased the heat transfer coefficient of the water bock. At a mass flow rate of 0.07 kg/s, the heat transfer coefficient has been enhanced by 12%, 18%, and 38% for nanofluids with 1%, 3.1%, and 6.8% nanoparticle concentrations, respectively, compared to the heat transfer coefficient of water. The heat transfer coefficient enhancement is similar for lower mass flow rates as well. As the turbulent flow becomes stronger, the heat transfer coefficient increases. Fig. 23 shows the influence of nanoparticle size on the heat transfer coefficient of the water block.

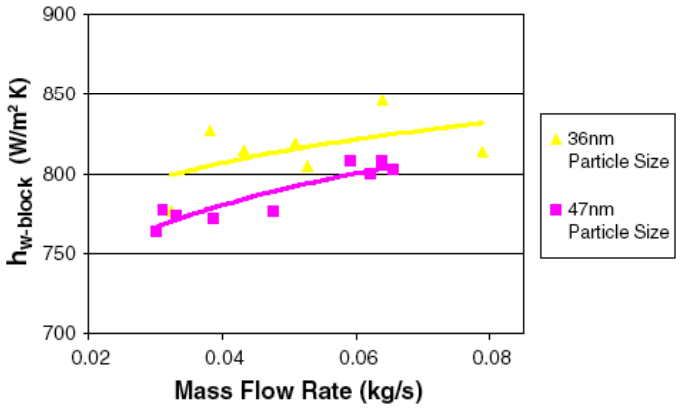

Fig. 23. Effect of particle size on $h_{w\text{-}block}$ for 6.8% nanoparticle volume concentration [27].

As one can see from Fig. 23, the smaller diameter nanoparticles (36 nm) produce a higher water block heat transfer coefficient than the large nanoparticle (47 nm) nanofluid.

2.8 Summary of Literature

Most of the research investigated in this chapter was for laminar or turbulent forced convection in a tube, because there is very little research on forced convection over a flat plate. The research summaries presented will not predict the outcomes of this research in terms of numerical results, but they may supply some indication as to what trends to expect.

All of the research studied in this chapter reported increases in heat transfer due to the addition of nanoparticles in the base fluid. To what degree and by what mechanism is still debatable. However, the following trends were in general agreement with all researchers:

- There is an enhancement in the heat transfer coefficient with increasing Reynolds number
- The heat transfer coefficient enhancement increases with decreasing nanoparticle size
- The heat transfer coefficient enhancement increases with increasing fluid temperature (more than just the base fluid alone)
- The heat transfer coefficient enhancement increases with increasing nanoparticle volume fraction

Some nanofluid research conflicts. Below are some explanations as to why there might be such a discrepancy between results:

A. Aggregation – It has been shown that nanoparticles tend to aggregate quite quickly in nanofluids, which can impact the thermal conductivity and the viscosity of the nanofluid. Not all researchers account for this whether it is through experimental or numerical research.

B. Unknown Nanoparticle Size Distribution – Researchers rarely report the size distribution of nanoparticles or aggregates—they only list one nanoparticle size—which could affect results. Many researchers don't measure the nanoparticles themselves, and rely on the manufacturer to report this information.

C. Differences in theory—Researchers have not agreed upon which heat transfer mechanisms are important, dominate, and how they should be accounted for in calculations. The discrepancy leads to different analyses and different results.

D. Different nanofluid preparation techniques—Depending on how the nanofluids are made, for instance whether it is by a one-step of two-step method, the dispersion of the nanofluids could be effected. Some researchers coat the nanoparticles to inhibit agglomeration, while others do not.

3. ANALYSIS

To simulate laminar, forced convection in nanofluid over a flate plate, equations for the continuity of fluid, continuity of nanoparticles, x-momentum, y-momentum, and energy must be derived. This is done in the following sections, assuming incompressible flow. The equations are then put into Mathematica to solve for the behavior of the nanofluid in terms of the velocity, volume fraction, temperature, and heat transfer coefficient.

3.1 Continuum Assumption

Before the nanofluid can be assumed to be a continuum, the Knudsen number needs to be calculated, which is given in Eq. (7).

$$Kn = \frac{\lambda}{d_p} \qquad \text{Eq. (7)}$$

The Knudsen number is the ratio of the water molecule mean free path to the nanoparticle diameter. The value of the Knudsen number indicates whether a medium can be assumed to be a continuum. When the Knudsen number is below 1, the continuum assumption is valid, and the system does not have to be analyzed on a molecule by molecule level. The mean free path in water is on the order of 0.3 nm and the nanoparticles are defined as being anywhere from 1 to 100 nm in diameter. This range leads to a Knudsen number of less than 0.3, which means that the continuum assumption is valid [17].

3.2 Scale Analysis of Nanoparticle Transport Mechanisms

Many heat transport mechanisms were presented in the introduction chapter. To determine which mechanisms to include in this analysis, it is helpful to find the time it takes a nanoparticle to diffuse a length equal to its diameter under the effect of each mechanism. Comparing the times will indicate which mechanisms are the most important, with the shortest time scale being more important than a longer time scale. The following thermophoresis, Brownian diffusion, and gravity calculations were first completed by Buongiorno [17] for a nanoparticle with a 100 nm diameter. Equation (8) gives the time scale for thermophoresis to take place.

$$\frac{d_p}{Ve_T} \sim 0.05s \qquad \text{where} \qquad Ve_T = -0.26\frac{k}{2k+k_p}\frac{\mu}{\rho}\bullet\frac{\nabla T}{T} \qquad \text{Eq. (8)}$$

In Eq. (8) Ve_T is the thermophoretic velocity [28], k is the thermal conductivity of the nanofluid, k_p is the thermal conductivity of the nanoparticle, μ is the viscosity of the nanofluid, ρ is the density of the nanofluid, and T is the temperature of the nanofluid. Equation (9) is the time scale for Brownian diffusion,

$$\frac{d_p^{\,2}}{D_B} \sim 0.002s, \qquad \text{Eq. (9)}$$

where D_B is the Brownian diffusion coefficient, which is given in Eq. (16). Equation (10) is the time scale for gravity, or how fast the nanoparticles will settle.

$$\frac{d_p}{Ve_g} \sim 6s \qquad \text{Eq. (10)}$$

In Eq. (10) Ve_g is the nanoparticle settling velocity due to gravity, which is the ratio of the buoyancy forces to the viscous forces, and is given in Eq. (11).

$$Ve_g = \frac{d_p{}^2(\rho_p - \rho)g}{18\mu} \qquad \text{Eq. (11)}$$

From this analysis, Brownian motion diffuses heat in about a thousandth of a second, while thermophoresis is an order of magnitude slower. Gravity takes 6 seconds, a very long time in comparison, and it will be left out of this analysis. Thermophoresis and Brownian diffusion will be taken into account. Prasher, Bhattacharya, and Phelan [12] performed a similar scale analysis and suggested that the effective thermal conductivity in nanofluids is mainly due to localized convection caused by Brownian motion.

3.3 Nanofluid Properties

Even though the nanofluid contains a very small volume fraction of nanoparticles, the nanoparticles will still affect the nanofluid's properties. The correlations for nanofluid properties are given in Eq. (12-15).

$$\rho(\phi) = \phi\rho_p + (1-\phi)\rho_{bf} \qquad (12)$$

$$c(\phi) = \frac{\phi c_p \rho_p + (1-\phi)c_{bf}\rho_{bf}}{\rho} \qquad (13)$$

$$\mu(\phi) = \mu_{bf}(1 + 39.11\phi + 533.9\phi^2) \quad \text{for alumina nanoparticles} \qquad (14)$$

$$k(\phi) = k_{bf}(1 + 7.47\phi) \quad \text{for alumina nanoparticles} \qquad (15)$$

As one can see, the equation for nanofluid density Eq. (12), simply follows the rule of mixtures. However, the equations for nanofluid viscosity and thermal

conductivity, Eq. (14-15), are completely based on experimental data, and they are only for alumina nanoparticles.

The nanoparticles also experience Brownian motion and thermophoresis, which are characterized by the coefficients in Eq. (16-17).

$$D_B = \frac{k_B T}{3\pi\mu d_p} \tag{16}$$

$$D_T = 0.26\left(\frac{k}{2k + k_p}\right)\left(\frac{\mu}{\rho}\right)\phi \tag{17}$$

Equation (16) is the Einstein-Stoke's equation for Brownian diffusion, and Eq. (17) is the thermal diffusion coefficient from McNab and Meisen [28].

3.4 Conservation of Mass for Nanofluid

Deriving the conservation of mass for the fluid produces an equation which will help solve for v, T, and ϕ. The conservation of mass states that the mass in a closed system must stay constant. Figure 24 depicts the control volume of fluid.

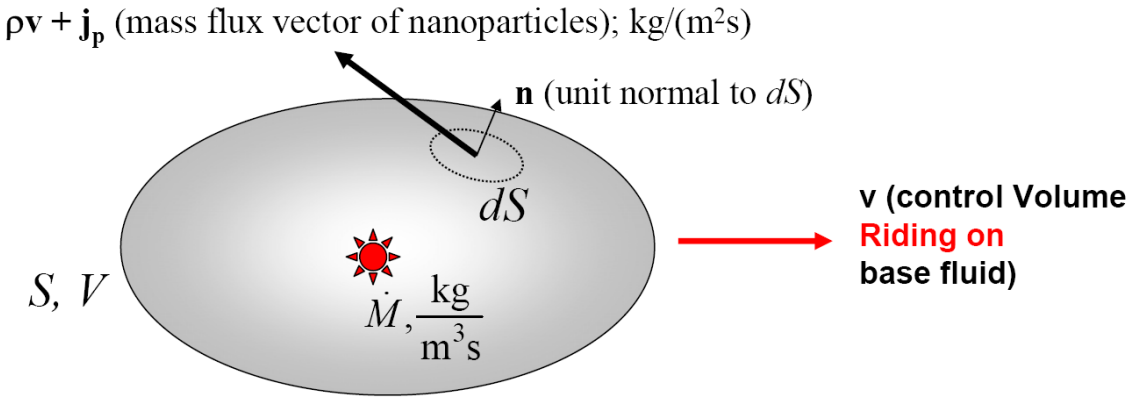

Fig. 24. Illustration of nanofluid control volume for continuity derivation [29].

In the figure, j_p is the nanoparticle mass flux due to the mass flux from Brownian diffusion and the mass flux due to thermophoresis, which is given by Eq. (18).

$$j_p = j_B + j_T = -\rho_p D_B \nabla \phi - \rho_p D_T \frac{\nabla T}{T} \tag{18}$$

where D_B and D_T are given by Eq. (16-17). Equation (19) is the mass balance for the control volume in Fig. 24, which is written in tensor notation.

$$\frac{D}{Dt}\int_V \rho dV = \int_V \dot{M} dV - \int_S \left(\rho \vec{v} + \vec{j}_p\right) \bullet \vec{n} dS \tag{19}$$

The mass generation term can be cancelled, which results in Eq. (20).

$$\frac{D}{Dt}\int_V \rho dV = -\int_S \left(\rho \vec{v} + \vec{j}_p\right) \bullet \vec{n} dS \tag{20}$$

The divergence theorem is used to convert the surface integral on the right hand side of the equation to a volume integral, and the density relation from Eq. (12) is inserted for density on the left hand side. Equation (20) is then broken up into Eq. (21-22) for the fluid and nanoparticles, respectively.

$$\frac{D}{Dt}\int_V (1-\phi)\rho_{bf} dV = -\int_V \nabla \bullet \rho \vec{v} dV \qquad \text{fluid} \tag{21}$$

$$\frac{D}{Dt}\int_V \rho_p \phi dV = -\int_V \nabla \bullet \vec{j}_p dV \qquad \text{nanoparticles} \tag{22}$$

Assuming that density terms on both sides of Eq. (21) are equal since the volume fraction of nanoparticles is so small, Eq. (21) reduces to Eq. (23), the final continuity equation for fluid.

$$\nabla \bullet \vec{v} = 0 \quad \text{continuity equation for fluid} \tag{23}$$

Notice that Eq. (23) is identical to the continuity equation for an incompressible fluid. After the integral of Eq. (22) has been evaluated, Eq. (24) is formed.

$$\rho_p \frac{D\phi}{Dt} = -\nabla \bullet \vec{j}_p \tag{24}$$

Realizing that $\frac{D}{Dt} = \frac{\partial}{\partial t} + \vec{v} \bullet \nabla$, and substituting Eq. (18) in to Eq. (24) results in Eq. (25), the final result for the continuity of nanoparticles.

$$\frac{\partial \phi}{\partial t} + \vec{v} \bullet \nabla \phi = \nabla \bullet \left(D_B \nabla \phi + D_T \frac{\nabla T}{T} \right) \text{ continuity for nanoparticles} \tag{25}$$

3.5 Conservation of Energy

Figure 25 shows an illustration of the control volume that will be used to derive the conservation of energy equation.

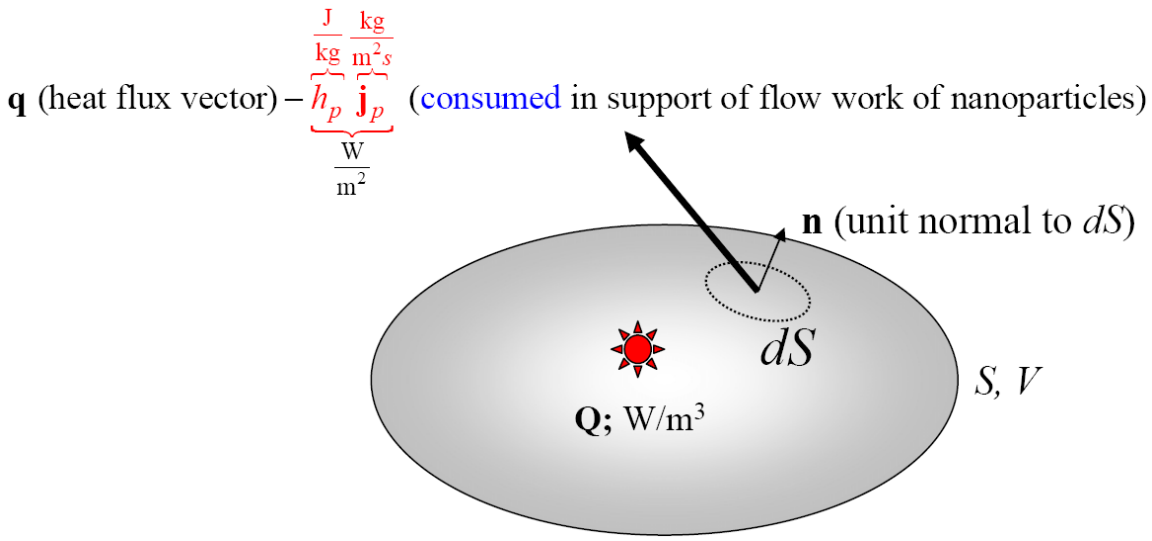

Fig. 25. Illustration of control volume for conservation of energy derivation [29].

The energy balance for the control volume in Fig. 25 is given by Eq. (26),

$$\frac{D}{Dt} \int_V cT\rho dV = \int_V Q dV - \int_S (\vec{q} - h_p \vec{j}_p) \bullet \vec{n} dS, \tag{26}$$

where enthalpy, $h_p=c_pT$, is a constant and $\vec{q} = -k\nabla T + h_p\vec{j}_p$. Canceling out the heat generation term and converting the surface integral to a volume integral using the divergence theorem, Eq. (27) is produced.

$$\frac{D}{Dt}\int_V cT\rho dV = -\int_V \nabla \bullet (\vec{q} - h_p\vec{j}_p)dV \tag{27}$$

Substituting in the expression for $\vec{q}$, $h_p = c_pT$, and $\vec{j}_p$, from Eq. (18), results in Eq. (28), which is the final energy equation.

$$\rho c\frac{DT}{Dt} = \nabla \bullet (k\nabla T) - \rho_p c_p D_B \nabla\phi \bullet \nabla T + \rho_p c_p D_T \frac{\nabla T \bullet \nabla T}{T} \tag{28}$$

3.6 Conservation of Momentum (Navier-Stokes)

A general form of the Navier-Stokes equation will be used, which is given in Eq. (29),

$$\rho\frac{D\vec{v}}{Dt} = -\nabla P - \nabla \bullet \tau, \tag{29}$$

where P is pressure, and τ is the stress. For this application, the stress tensor is given by Eq. (30).

$$\tau = -\mu[\nabla\vec{v} + (\nabla\vec{v})^T] \tag{30}$$

Putting Eq. (30) and $\frac{D}{Dt} = \frac{\partial}{\partial t} + \vec{v} \bullet \nabla$ into Eq. (29) results in Eq. (31), the form of Navier-Stokes that will be used for this analysis.

$$\rho\left(\frac{\partial\vec{v}}{\partial t} + \vec{v} \bullet \nabla\vec{v}\right) = -\nabla P - \nabla \bullet \mu\left[\nabla\vec{v} + (\nabla\vec{v})^T\right] \tag{31}$$

Equation (31) is simply the conservation of momentum for an incompressible, Newtonian fluid.

3.7 Equation Summary

Table 1 displays the equations that have been derived to characterize the behavior of the nanofluid.

Table. 1. Summary of equations in tensor form.

$\nabla \bullet \vec{v} = 0$	Continuity Equation for fluid
$\frac{\partial \phi}{\partial t} + \vec{v} \bullet \nabla \phi = \nabla \bullet \left(D_B \nabla \phi + D_T \frac{\nabla T}{T} \right)$	Continuity Equation for nanoparticles
$\rho \left(\frac{\partial \vec{v}}{\partial t} + \vec{v} \bullet \nabla \vec{v} \right) = -\nabla P - \nabla \bullet \mu \left[\nabla \vec{v} + (\nabla \vec{v})^T \right]$	Navier-Stokes
$\rho c \frac{DT}{Dt} = \nabla \bullet (k \nabla T) - \rho_p c_p D_B \nabla \phi \bullet \nabla T + \rho_p c_p D_T \frac{\nabla T \bullet \nabla T}{T}$	Energy Equation

There are four equations for four unknowns: $\vec{v}$, T, ϕ, and P. The continuity equations are strongly coupled; $\vec{v}$ depends on ϕ because of viscosity, ϕ depends on T because of thermophoresis, T depends on ϕ because of thermal conductivity, Brownian diffusion, and thermophoresis, ϕ, and T depend on $\vec{v}$.

3.8 Boundary Layer Scale Analysis

The first step in completing the boundary layer analysis is to take the equations in Table 1 out of tensor notation, which is shown in Eq. (32-36) below. Figure 26 shows the u, v, x, and y coordinate system with respect to the plate.

Continuity Equation for Fluid Eq. (32)

$$\frac{\partial u}{\partial x}+\frac{\partial v}{\partial y}=0$$

Continuity Equation for Nanoparticles Eq. (33)

$$u\frac{\partial \phi}{\partial x}+v\frac{\partial \phi}{\partial y}=\frac{\partial}{\partial x}\left(D_B\frac{\partial \phi}{\partial x}+\frac{D_T}{T}\frac{\partial T}{\partial x}\right)+\frac{\partial}{\partial y}\left(D_B\frac{\partial \phi}{\partial y}+\frac{D_T}{T}\frac{\partial T}{\partial y}\right)$$

Momentum Equation in the x Direction Eq. (34)

$$\rho\left(u\frac{\partial u}{\partial x}+v\frac{\partial u}{\partial y}\right)=-\frac{\partial P}{\partial x}+2\frac{\partial}{\partial x}\left[\mu\left(\frac{\partial u}{\partial x}\right)\right]+\frac{\partial}{\partial y}\left[\mu\left(\frac{\partial u}{\partial y}+\frac{\partial v}{\partial x}\right)\right]$$

Momentum Equation in the y Direction Eq. (35)

$$\rho\left(u\frac{\partial v}{\partial x}+v\frac{\partial v}{\partial y}\right)=-\frac{\partial P}{\partial y}+2\frac{\partial}{\partial y}\left[\mu\left(\frac{\partial v}{\partial y}\right)\right]+\frac{\partial}{\partial x}\left[\mu\left(\frac{\partial u}{\partial y}+\frac{\partial v}{\partial x}\right)\right]$$

Energy Equation Eq. (36)

$$\rho c\left(u\frac{\partial T}{\partial x}+v\frac{\partial T}{\partial y}\right)=\frac{\partial}{\partial x}\left(k\frac{\partial T}{\partial x}\right)+\frac{\partial}{\partial y}\left(k\frac{\partial T}{\partial y}\right)+\rho_p c_p D_B\left[\left(\frac{\partial \phi}{\partial x}\right)\left(\frac{\partial T}{\partial x}\right)+\left(\frac{\partial \phi}{\partial y}\right)\left(\frac{\partial T}{\partial y}\right)\right]+\frac{\rho_p c_p D_T}{T}\left[\left(\frac{\partial T}{\partial x}\right)^2+\left(\frac{\partial T}{\partial y}\right)^2\right]$$

The purpose of the boundary layer analysis is to simplify Eq. (32-36). By doing a scale analysis on the boundary layer, the terms that will be very small can be identified and discarded from the equations, simplifying the analysis. Figure 26 depicts the fluid flow with respect to the scale variables that will be used.

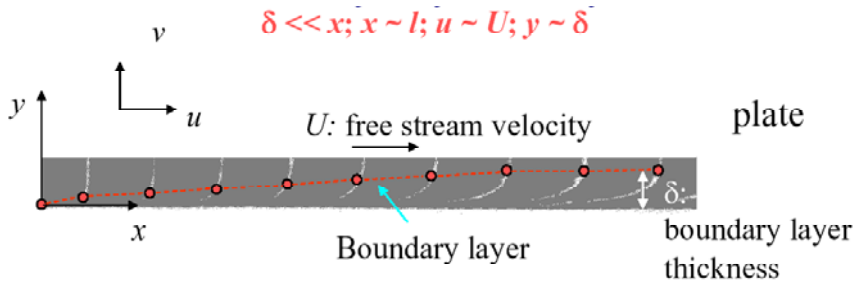

Fig. 26. Illustration of similarity variables [29].

In Fig. 26, the boundary layer thickness, δ, is assumed to be much less than the x, the distance along the plate. x is on the same order of magnitude as l, the length of the plate, the velocity in the x direction, u, is on the same order of magnitude as U, the free stream velocity, and the velocity in the y direction, y, is assumed to very small, on the same order of magnitude as the boundary layer thickness, δ. These similarity variables will be put into Eq. (32-36). The continuity equation for fluid will be analyzed first in Eq. (37).

$$\frac{\partial u}{\partial x}+\frac{\partial v}{\partial y}=0 \qquad \text{Eq. (37)}$$

$$\frac{U}{l}+\frac{v}{\delta}=0$$

Since U and l are on the same order of magnitude, and v and δ are on the same order of magnitude, neither term in the blue boxes approach zero, and no terms can be cancelled. Therefore the continuity equation for fluid stays the same. Equation (38) shows the scale analysis for the continuity equation for nanoparticles.

$$u\frac{\partial \phi}{\partial x}+\quad v\frac{\partial \phi}{\partial y}\quad =\frac{\partial}{\partial x}\left(D_B\frac{\partial \phi}{\partial x}+\frac{D_T}{T}\frac{\partial T}{\partial x}\right)+\frac{\partial}{\partial y}\left(D_B\frac{\partial \phi}{\partial y}+\frac{D_T}{T}\frac{\partial T}{\partial y}\right) \qquad \text{Eq. (38)}$$

$$U\left[\frac{\phi}{l}\right] \qquad \frac{U}{l}\delta\frac{\phi}{\delta}\Rightarrow U\frac{\phi}{l} \qquad \frac{D_B\phi}{l^2} \qquad \frac{D_T}{l^2} \qquad \frac{D_B\phi}{\delta^2} \qquad \frac{D_T}{\delta^2}$$

Moving from left to right, the first term cannot be canceled because it does not approach zero. For the second term, the free stream velocity is divided by the length of the plate, which cancels the length component of the velocity and it is

then multiplied by δ, which is of the same order as the y. Canceling out δ results in a term which cannot be neglected. If term three is compared to term five, term three will be very small, and it can be canceled, which is why the box is pink. If term four is compared to term six, term four will be much smaller, and it can be canceled. Canceling out these terms leaves Eq. (39).

$$u\frac{\partial \phi}{\partial x}+v\frac{\partial \phi}{\partial y}=\frac{\partial}{\partial y}\left(D_B\frac{\partial \phi}{\partial y}\right)+\frac{\partial}{\partial y}\left(\frac{D_T}{T}\frac{\partial T}{\partial y}\right) \qquad \text{Eq. (39)}$$

The next scale analysis will be performed on Eq. (34), the momentum equation in the x direction. This equation is longer, so due to page space requirements, the scale analysis will be done in two parts.

$$\underset{\frac{U^2}{l}}{\rho u\frac{\partial u}{\partial x}}+\underset{\frac{U}{l}\delta\frac{\phi}{\delta}\Rightarrow U\frac{\phi}{\delta}}{\rho v\frac{\partial u}{\partial y}}=-\frac{\partial P}{\partial x}+2\frac{\partial}{\partial x}\left[\mu\left(\frac{\partial u}{\partial x}\right)\right]+\underset{\frac{U}{\delta}}{\frac{\partial}{\partial y}\left[\mu\left(\frac{\partial u}{\partial y}+\frac{\partial v}{\partial x}\right)\right]} \qquad \text{Eq. (40)}$$

$$\frac{U}{l}\delta\frac{1}{l}=\frac{U}{\delta}\left(\frac{\delta}{l}\right)^2$$

From Eq. (40), the first two terms cannot be canceled because neither has a very small order. The second two terms represent the scale analysis for $\left(\frac{\partial u}{\partial y}+\frac{\partial v}{\partial x}\right)$. The third term cannot be canceled, but the fourth term is multiplied by the ratio of the boundary layer thickness to the length of the plate, which will approach a very small value. Therefore, this term cancels. Taking out the last term gives Eq. (41). The remainder of the terms will be analyzed.

$$\rho\left(u\frac{\partial u}{\partial x}+v\frac{\partial u}{\partial y}\right)=-\frac{\partial P}{\partial x}+2\frac{\partial}{\partial x}\underset{\frac{1}{l}\mu\frac{U}{l}=\frac{\mu U}{l^2}}{\left[\mu\left(\frac{\partial u}{\partial x}\right)\right]}+\underset{\frac{1}{\delta}\mu\frac{U}{\delta}=\frac{\mu U}{\delta^2}=\frac{\mu U}{l^2}\left(\frac{l}{\delta}\right)^2}{\frac{\partial}{\partial y}\left[\mu\left(\frac{\partial u}{\partial y}\right)\right]} \qquad \text{Eq. (41)}$$

If the two terms in Eq. (41) are compared, the term on the right is larger by the value of $\left(\frac{l}{\delta}\right)^2$, which will be very large and allow for the term on the left to be discarded. Also, $-\frac{\partial P}{\partial x}$ will be dropped because this analysis is for flow over a flat plate, so there should not be a pressure drop over the length of the plate. The result from these reductions is Eq. (42), the final x momentum equation.

$$\rho\left(u\frac{\partial u}{\partial x}+v\frac{\partial u}{\partial y}\right)=\frac{\partial}{\partial y}\left[\mu\left(\frac{\partial u}{\partial y}\right)\right] \qquad \text{Eq. (42)}$$

As in the analysis of many fluid flows, the y momentum equation will be negligible. All of the terms in the y momentum equation are multiplied by some order of $\frac{\delta}{l}$, which is extremely small. The last scale analysis will be for the energy equation, which is shown in Eq. (43).

Eq. (43)

$$\rho c\left(u\frac{\partial T}{\partial x}+v\frac{\partial T}{\partial y}\right)=\frac{\partial}{\partial x}\left(k\frac{\partial T}{\partial x}\right)+\frac{\partial}{\partial y}\left(k\frac{\partial T}{\partial y}\right)+\rho_p c_p D_B\left[\left(\frac{\partial \phi}{\partial x}\right)\left(\frac{\partial T}{\partial x}\right)+\left(\frac{\partial \phi}{\partial y}\right)\left(\frac{\partial T}{\partial y}\right)\right]+\frac{\rho_p c_p D_T}{T}\left[\left(\frac{\partial T}{\partial x}\right)^2+\left(\frac{\partial T}{\partial y}\right)^2\right]$$

$$\frac{UT}{l} \quad \frac{U}{l}\delta\frac{T}{\delta}=\frac{UT}{l} \quad \frac{kT}{l^2} \quad \frac{kT}{\delta^2} \quad \frac{\phi T}{l^2} \quad \frac{\phi T}{\delta^2} \quad \frac{T^2}{l^2} \quad \frac{T^2}{\delta^2}$$

From left to right, the first two terms must be kept because neither ratio become small. Comparing the third and fourth terms it can be seen that the fourth term will become much larger, since it is divided by such a small number, δ^2. The same condition holds true for terms five and six and seven and eight.

Table 2. displays a summary of the governing equations for this analysis.

Table 2. Summary of final governing equations.

$\frac{\partial u}{\partial x}+\frac{\partial v}{\partial y}=0$	Continuity for Fluid
$u\frac{\partial \phi}{\partial x}+v\frac{\partial \phi}{\partial y}=\frac{\partial}{\partial y}\left(D_B\frac{\partial \phi}{\partial y}\right)+\frac{\partial}{\partial y}\left(\frac{D_T}{T}\frac{\partial T}{\partial y}\right)$	Continuity for Nanoparticles
$\rho\left(u\frac{\partial u}{\partial x}+v\frac{\partial u}{\partial y}\right)=\frac{\partial}{\partial y}\left[\mu\left(\frac{\partial u}{\partial y}\right)\right]$	x-momentum
$\rho c\left(u\frac{\partial T}{\partial x}+v\frac{\partial T}{\partial y}\right)=\frac{\partial}{\partial y}\left(k\frac{\partial T}{\partial y}\right)+\rho_p c_p D_B\left(\frac{\partial \phi}{\partial y}\right)\left(\frac{\partial T}{\partial y}\right)+\frac{\rho_p c_p D_T}{T}\left(\frac{\partial T}{\partial y}\right)^2$	Energy

In the above equations, ρ, μ, c, and k are all functions of the nanoparticle volume concentration. This makes the equations highly nonlinear.

3.9 Mathematica Program Development

Since the equations in Table 2 are highly nonlinear PDEs, the finite difference method [30] is used to reduce the set of equations to nonlinear ODEs, which can be put into a Mathematica solver. In the method, all of the derivatives with respect to space variable x are left as derivatives, and all of the derivatives with respect to space variable y are written in finite difference form. This leaves ODEs. The equations for central finite difference are given in Eq. (44-45).

$$\frac{dv}{dy}=\frac{v_{i+1}-v_{i-1}}{2\Delta y} \qquad \text{Eq. (44)}$$

$$\frac{d^2v}{dy^2}=\frac{v_{i+1}-2v_i+v_{i-1}}{\Delta y^2} \qquad \text{Eq. (45)}$$

Equation (44) is for a first order derivative and Eq. (45) is for a second order derivative. In both equations, v is a function of y, and Δy is the step size. Every differential term with respect to y will be put into the form of Eq. (44) or Eq. (45). For instance the continuity equation for fluid will become Eq. (46).

$$\frac{du_i}{dx} + \frac{v_{i+1} - v_{i-1}}{2\Delta y} = 0 \qquad \text{Eq. (46)}$$

The equations are put into Mathematica and solved using an ODE solver. Figure 27 shows the convention for labeling the nodes in the Mathematica program.

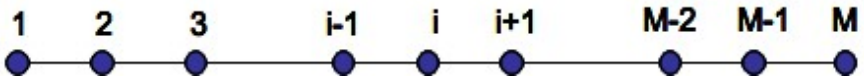

Fig. 27. Illustration of node labeling convention.

In Fig. 27, the node 1 is next to the plate, and M is at the surface of the fluid. Table 3. shows the boundary condition variables that are used to solve the systems of ODEs.

Table 3. Mathematica program variable descriptions.

TB	bottom temperature
UB	u bottom velocity
VB	v bottom velocity
FB	bottom volume fraction of nanoparticles
TT	top temperature
UT	u top velocity
VT	v top velocity
FT	top volume fraction of nanoparticles
W	nanofluid thickness in y direction
L	length of plate

The Mathematica program developed from this analysis is shown in Appendix A.

4. RESULTS

The characteristics, fluid flow development, and heat transfer coefficient for ethylene glycol/alumina and water/alumina nanofluid have been studied in detail. The nanoparticle diameter size, nanoparticle volume fraction, fluid temperature, and free stream velocity have been varied to observe their effects. Unless otherwise noted, the following analyses are for the base conditions listed in Table 4.

Table 4. Base conditions for analyses.

Nanofluid Type	**Ethylene Glycol/Alumina**	**Water/Alumina**
Base Fluid Density	1103.7 kg/m^3	997.009 kg/m^3
Base Fluid Thermal Conductivity	0.255 W/mK	0.613 W/mK
Base Fluid Viscosity	1.07 ×10^{-2} Ns/m^2	855×10^{-6} Ns/m^2
Base Fluid Heat Capacity	2460 J/kgK	4179 J/kgK
Nanoparticle Thermal Conductivity	46 W/mK	46 W/mK
Nanoparticle Density	3970 kg/m^3	3970 kg/m^3
Nanoparticle Heat Capacity	7160 J/kgK	760 J/kgK
Top Nanoparticle Concentration	0.00	0.00
Bottom Nanoparticle Concentration	0.01	0.01
Nanofluid Top Temperature	300 K	300 K
Nanofluid Bottom Temperature	320 K	320 K
Free Stream Velocity	10 m/s	10 m/s
Plate Length	3 m	30 m
Fluid Depth	0.01 m	0.01 m

In Table 4, parameters labeled “Top” correspond to values that are at the surface of the nanofluid and parameters labeled “Bottom” correspond to parameters at the bottom of the nanofluid, next to the plate. Except for the base fluid properties, all other parameters, except the length of the plate, which will be explained in further detail later, are the same.

4.1 Basic Nanofluid Characteristics

4.1.1 Nanoparticle Volume Fraction Distribution

The nanoparticle distribution is effected by the size of the nanoparticles. As the size of the nanoparticle is reduced, the nanoparticles become more dispersed throughout the fluid, which can be seen in Fig. 28, for water.

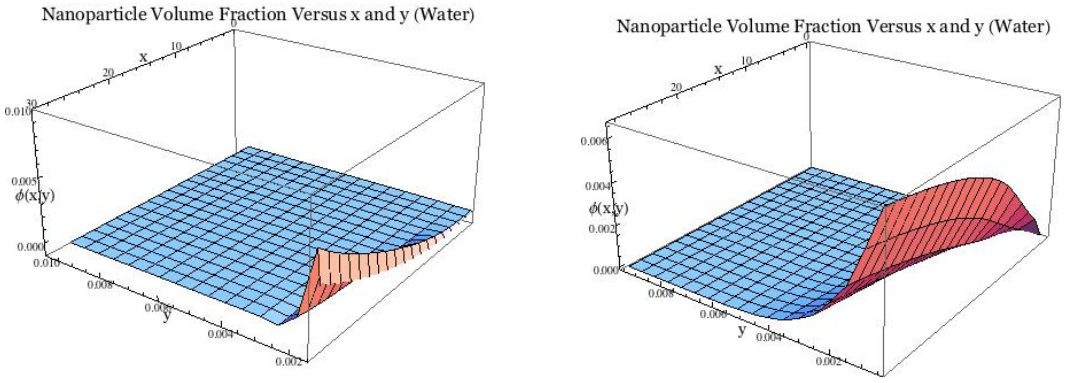

a) d_p = 10.0 nm b) d_p = 0.001 nm

Fig. 28 a) Nanoparticle volume fraction with nanoparticle diameters of 10 nm. b) Nanoparticle volume fraction with nanoparticle diameters of 0.001 nm.

Figure 28 a) is for a nanoparticle size of 10 nm and Fig. 28 b) is for a nanoparticle size of 0.001 nm. The smallest nanoparticle is of the order of 0.1 nm, and the case of 0.001 nm in Fig. 28 b) is used in this analysis for producing a noticeable difference in illustrating the size effect of nanoparticles. As the nanoparticle size is decreased, Brownian motion and thermophoresis take more effect because the nanoparticle size has approached the size of liquid molecules, making it easier for the nanoparticles to stay suspended. Both the alumina/ethylene glycol and alumina/water nanofluids exhibit this behavior.

The nanoparticle distribution is also slightly effected by the temperature at the base. As the temperature of the base increases, so does the nanoparticle

concentration next to the plate. However, the effect of the temperature increase on the nanoparticle volume concentration distribution is slight. There is about 0.1% increase in nanoparticle dispersion for every 60 K the temperature of the plate is increased.

As the free stream velocity is decreased, the nanoparticle volume fraction increases next to the plate, meaning that the nanoparticles tend to settle more at lower free stream velocities. This effect was best seen when the diameter of the particle was 0.001 nm. Figure 29 a) shows when the free stream velocity is 10 m/s and Fig. 29 b) shows when the free stream velocity is 1 m/s. Alumina/water nanofluid is used in the figure.

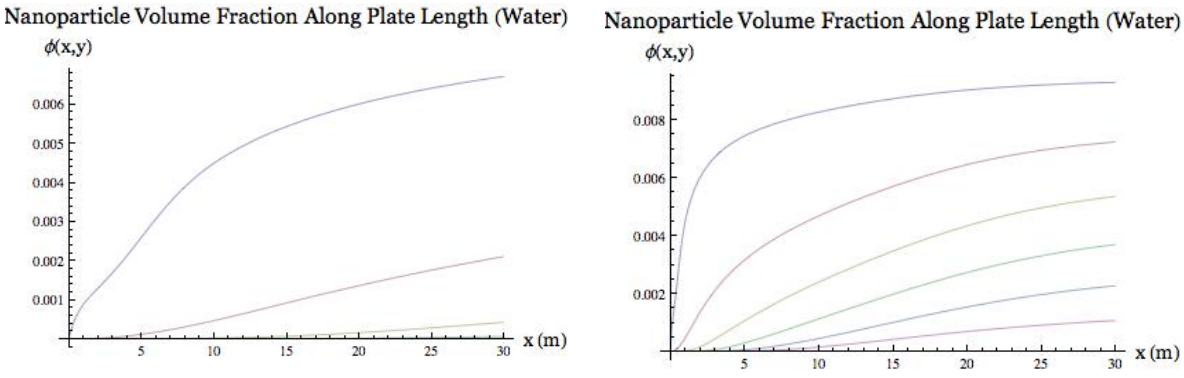

a) b)

Fig. 29 a) Nanoparticle volume fraction along length of plate for nanoparticle diameters of 0.001 m at a 10 m/s free stream velocity. b) Nanoparticle volume fraction along length of plate for nanoparticle diameters of 0.001 m at a 1 m/s free stream velocity.

Figure 29 shows the nanoparticle volume fraction as the nanofluid moves down the flat plate. The different lines represent the nanoparticle volume fraction as the nanofluid gets farther away from the plate, with the y direction going into the paper. The top lines are the closest to the plate and the lower lines are closer to

the surface of the nanofluid. As can be seen in Fig. 29 a), the nanoparticles start to settle at the bottom of the plate farther down the plate than the nanoparticles in Fig. 29 b).

4.1.2 Temperature Distribution

The temperature distribution is mostly dependent on the nanoparticle size, which is shown in Fig. 30.

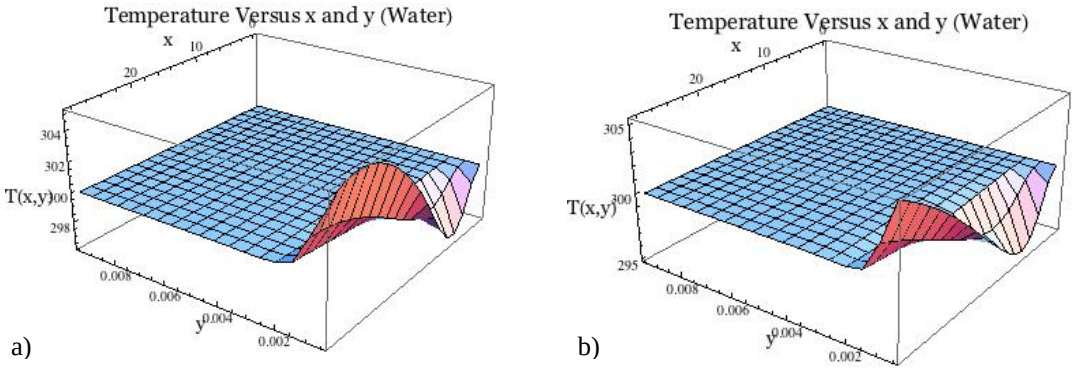

Fig. 30. a) Temperature distribution for alumina/water nanofluid with 10 nm diameter particles. b) Temperature distribution for alumina/water nanofluid with 0.001 nm diameter particles.

Figure 30 a) shows the temperature distribution for alumina/water nanofluid with 10 nm diameter particles and Fig. 30 b) shows the temperature distribution for water/alumina nanofluid with 0.001 nm diameter particles. Again, such a small particle diameter in Fig. 30 b) is chosen because, at this size, the differences in the temperature distribution compared to Fig. 30 a) are very pronounced. As the particle diameter is decreased, the particles maintain their distribution in the fluid longer along the plate length. This can be seen as the temperature next to the plate does not rise as high in Fig. 30 b) as in Fig. 30 a). Increasing the free

stream velocity does not have much effect on the temperature distribution, and it only increases the length it takes for the velocity profile to become fully developed.

4.1.3 Velocity in the v Direction

Figure 31 a) and 31 b) show the velocity profile in the y direction for ethylene glycol/alumina nanofluid.

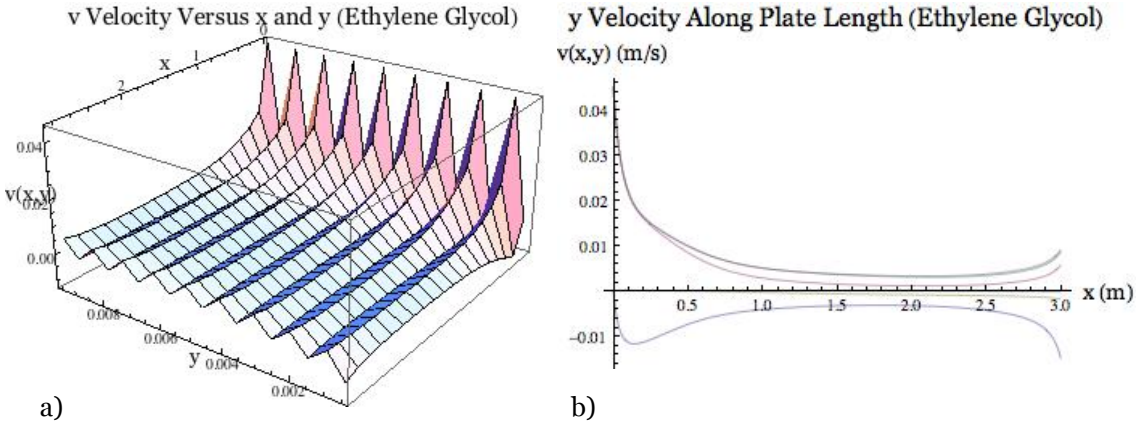

a) b)

Fig. 31. a) 3-D plot of velocity behavior in the y direction for alumina/water nanofluid. b) 2-D plot of velocity behavior in the y direction for alumina/water nanofluid.

As can be seen in Fig. 31 a), the v velocity is fluctuating, but the fluctuation becomes less as the nanofluid travels down the length of the plate. Figure 31 b) shows a 2-D plot of the velocity profile in the y direction. The different streamlines are the v velocity profiles along the y direction of the fluid. From the figure, some of the velocity profiles go negative, but they balance out with the positive streamlines, producing a zero mean v velocity. Regular fluids also exhibit

this behavior. The same trend is true for the alumina/water nanofluid, which is shown in Fig. 32 a) and b).

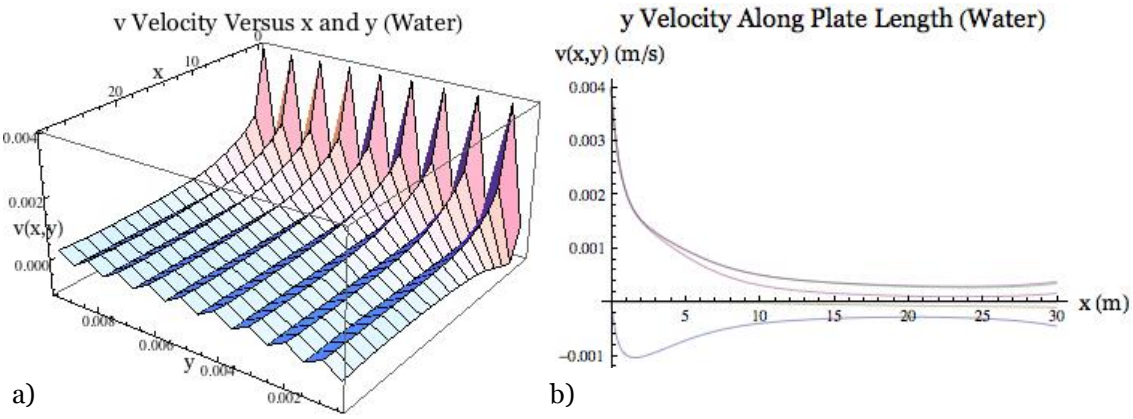

Fig. 32. a) 3-D plot of velocity behavior in the y direction for alumina/water nanofluid b) 2-D plot of velocity behavior in the y direction for alumina/water nanofluid.

4.2 Variables in Velocity Profile Development

4.2.1 Varying the Length of the Plate

The alumina/water and alumina/ethylene glycol nanofluids were evaluated in the Mathematica program under the same conditions, except for the length of the plate. When W, the thickness of the water above the plate is 0.01 m, and the properties for ethylene glycol are used in the Mathematica program, the program can handle plate lengths up to 3 m. The aspect ratio of the width to the length of the nanofluid determines the computational domain of the program. At a plate length of 3 m, the velocity profile of the alumina/ethylene glycol nanofluid is fully developed. However, when the properties for water are entered into the Mathematica program, the program can handle a plate length up to 35 m. At a plate length of 3 m, the water-based nanofluid is not fully developed. The plots of

the velocity along a 3 m long plate are shown in Fig. 33. Figure 33 a) shows the velocity profile for ethylene glycol/alumina nanofluid and Fig. 33 b) shows the velocity profile for water/alumina.

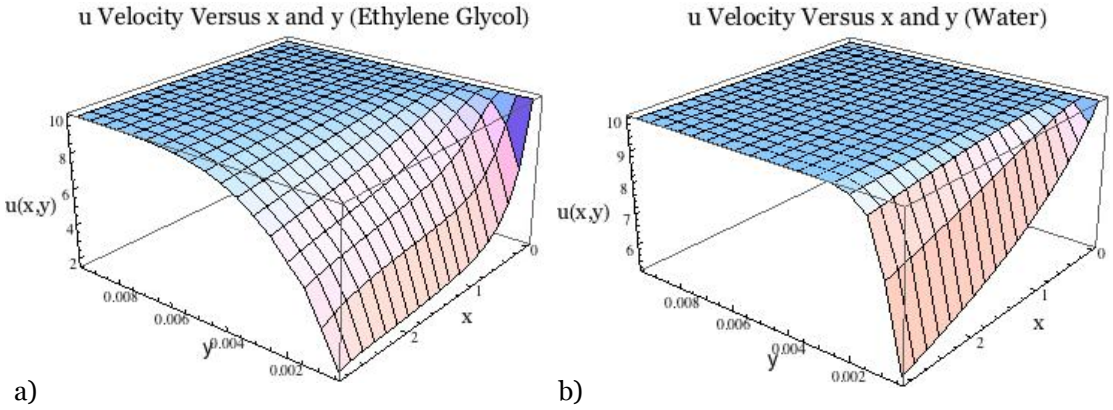

a) b)

Fig. 33. a) Fully developed velocity profile for alumina/ethylene glycol nanofluid over a 3 m plate. b) Developing velocity profile for alumina/water nanofluid over a 3 m plate.

Figure 34 shows the velocity along the length of the plate in a two-dimensional plot for the same conditions.

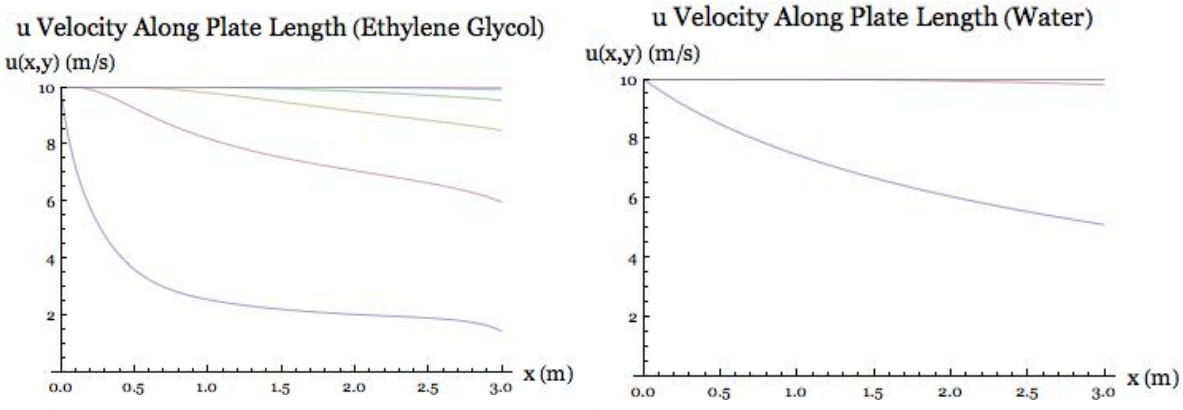

a) b)

Fig. 34. a) Fully developed 2-D velocity profile for alumina/ethylene glycol nanofluid over a 3 m long plate. b) Developing 2-D velocity profile for alumina/water nanofluid over a 3 m long plate.

In the plot, the streamlines are the velocity profiles of the nanofluid as it goes farther downstream. The top streamlines are the nanofluid velocities closer to the

entrance, and the lower streamlines are for the fluid flow towards the end of the plate. The bottom streamline is fully developed in Fig. 34 a), while it is still developing in Fig. 34 b). The velocity profile for the water-based nanofluid is fully developed by 30 m along the length of the plate, which is shown in Fig. 35.

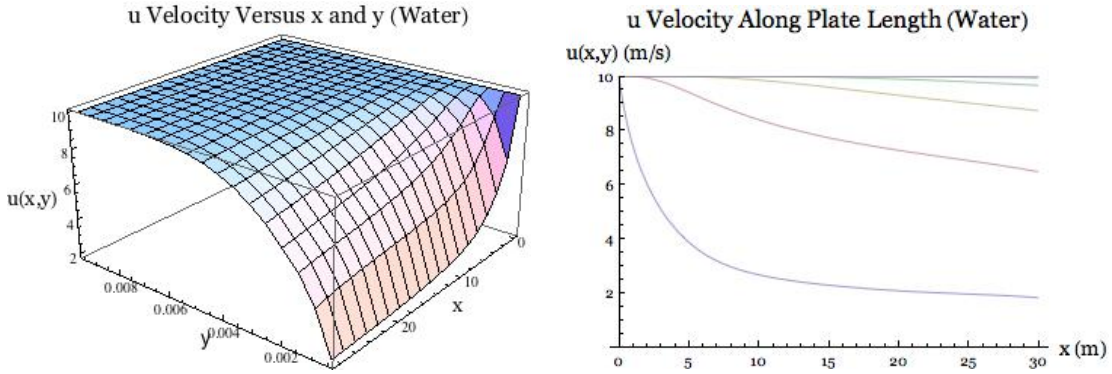

a) b)

Fig. 35. a) 3-D fully developed velocity profile for alumina/water nanofluid. b) 2-D fully developed velocity profile for alumina/water nanofluid.

It should be noted that these results are for a free stream velocity of 10 m/s. As velocity is increased, the length of plate that the Mathematica program can tolerate can be increased as well, for both types of nanofluids. The plate length can also be increased when the nanofluid thickness in the y domain is increased.

4.2.2 Varying Velocity

For both types of nanofluids, as the velocity is increased, the velocity profile requires a longer plate distance to become fully developed. This is because the boundary layer is being analyzed. Since both fluids exhibit this trend, only

results from the ethylene glycol mixture will be presented. Table 5 displays the increase in development region length with increasing free stream velocity for ethylene glycol.

Table 5. Increase in development region length with increasing free stream velocity for alumina/ethylene glycol nanofluid.

Velocity Profile with x=3	Fully Developed Velocity Profile
u = 10 m/s, x=3 m 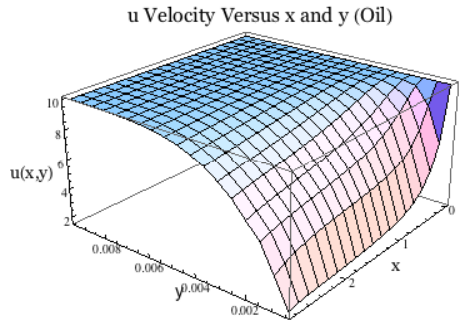	The plot to the left is fully developed.
u = 20 m/s, x=3 m 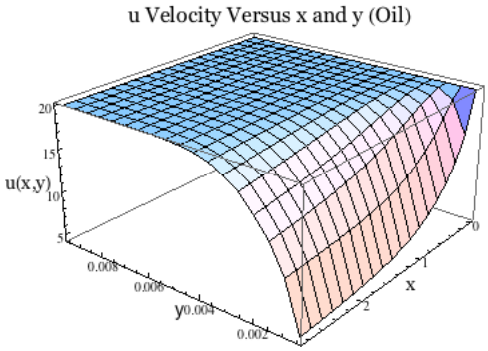	u = 20 m/s, x=6 m 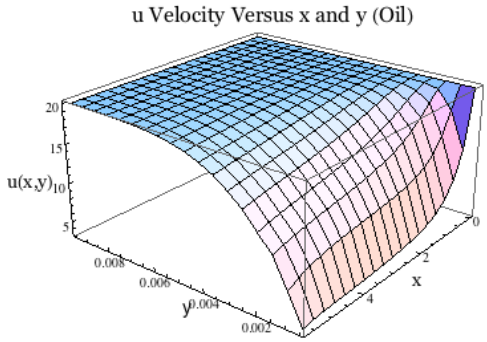
u = 30 m/s, x=3 m 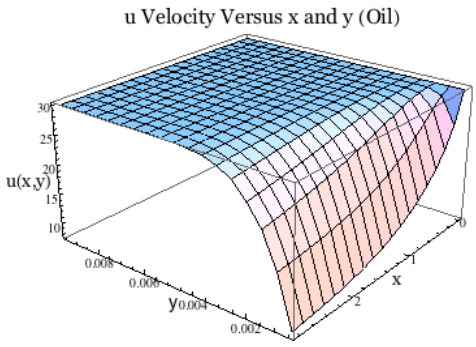	u = 30 m/s, x=9 m 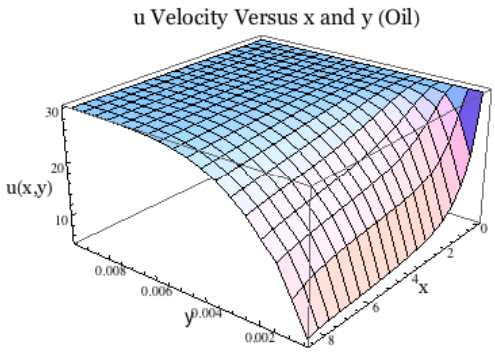

In the left column of Table 5, the free stream velocity is increased as the plate length is kept the same. As the velocity gets greater, the flow appears to be less developed. The column to the right shows the velocity profile as the free stream velocity increases and the plate length increases. As can be seen, all of the profiles in the right column appear to be fully developed. The development length and the free stream velocity seem to have a linear relationship, $3u = 10x$.

4.3 Variables of the Heat Transfer Coefficient

4.3.1 Varying Nanofluid Temperature

With the way the Mathematica program is written, the user can specify the temperature of the nanofluid at the top surface of the boundary layer and the temperature at the plate surface. Different combinations of the two temperatures had some effect on the heat transfer coefficient of the nanofluids. The results of the alumina/ethylene glycol nanofluid are is shown in Fig. 36.

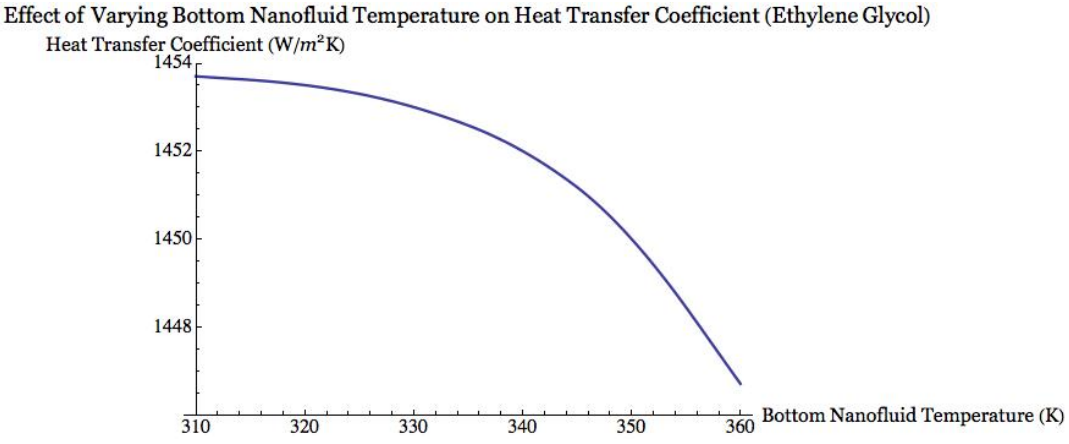

Fig. 36. Effect of varying nanofluid temperature at the bottom of the nanofluid on the heat transfer coefficient (temperature at the top is held constant at 300K).

In Fig. 36, the temperature at the top of the nanofluid was held constant at 300 K, while the temperature at the bottom of the nanofluid was varied. The heat transfer coefficient ranged from around 1447 to 1454, a 7 W/m²K difference, over a 50 K change in temperature. There is definitely an effect due to the temperature change, but it is very slight. The temperature at the top of the nanofluid was also varied, as the temperature at the bottom of the nanofluid was held constant at 360 K, and the results are shown in Fig. 37.

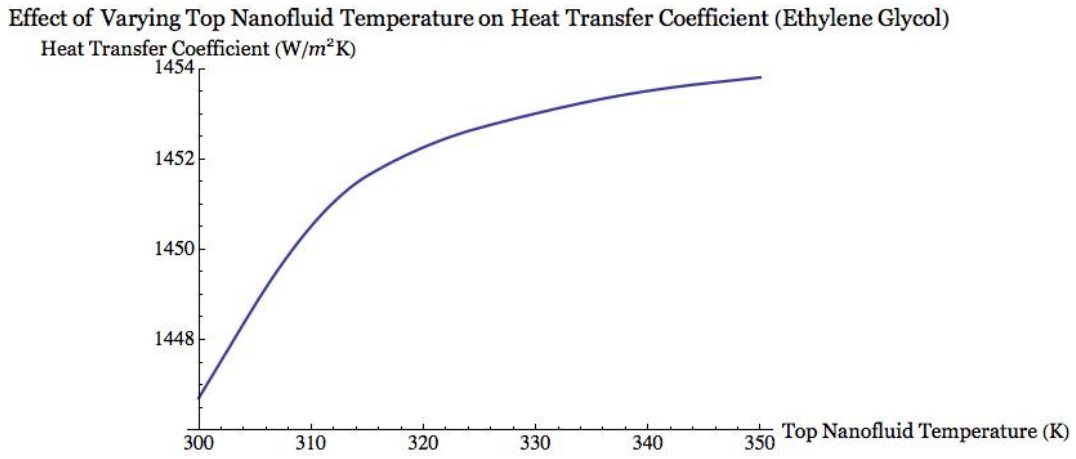

Fig. 37. Effect of varying nanofluid temperature at the top of the nanofluid on the heat transfer coefficient (temperature at the bottom is held constant at 360K).

Figure 37 exhibits the same trend as in Fig. 36, but in reverse. The change in heat transfer coefficient has the same range, 1447 to 1454 W/m²K, which is expected, since the heat transfer depends on the temperature difference and not the absolute temperatures on the bottom or top of the nanofluid.

As one can see, the change in heat transfer coefficient due to changing the fluid temperature is slight. When the same procedure was performed with the alumina/water nanofluid, there was no observable change in the heat transfer coefficient. Even when the nanoparticle size was reduced, there was no change in

the heat transfer coefficient due to changing the temperatures for the alumina/water nanofluid. This discrepancy must be due to the different properties of the base fluid, as all other parameters such as nanoparticle size and concentration were held constant.

4.3.2 Varying Nanoparticle Size

As the nanoparticle size is decreased, the heat transfer coefficient dramatically increases which is shown in Fig. [38-39].

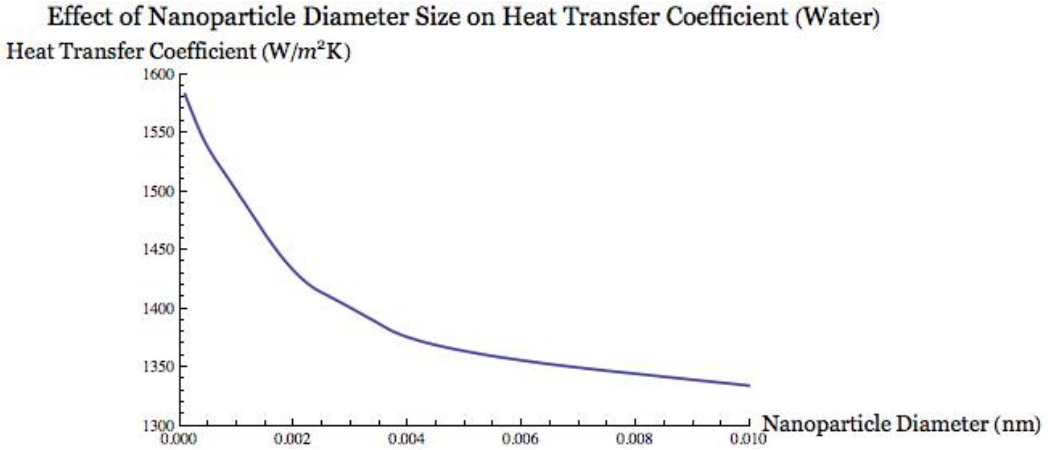

Fig. 38. Effect of nanoparticle diameter on the heat transfer coefficient for water/alumina nanofluid.

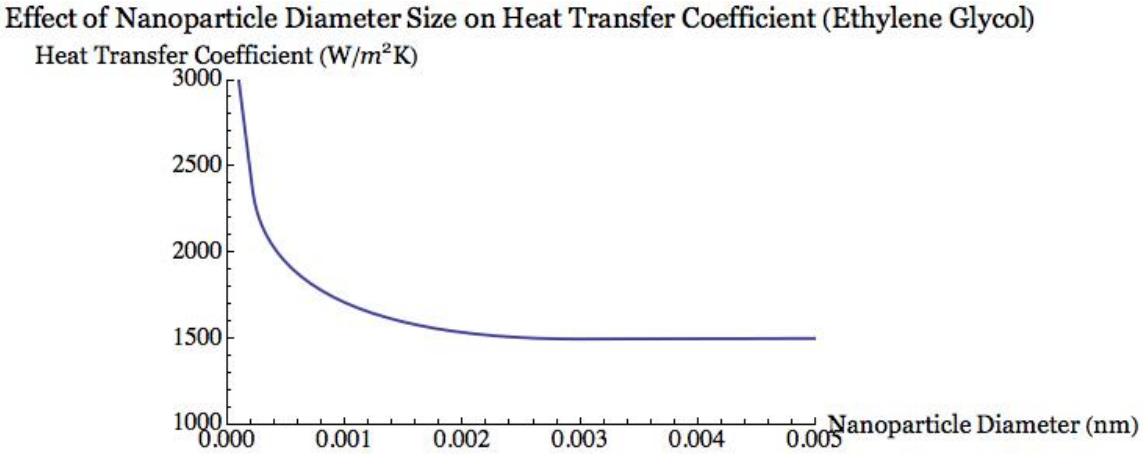

Fig. 39. Effect of nanoparticle diameter on the heat transfer coefficient for ethylene glycol/alumina nanofluid.

In Fig. 38-39, the heat transfer coefficient levels off at larger nanoparticle diameters than what is shown in the figures. The significant jump in the heat transfer coefficient in both figures is due to the fact that the nanoparticles are small enough that they are of comparable size to the mean free path of molecules, which helps them stay suspended and in motion, which would result in an increased Brownian motion and thermophoresis. Once again, the small particles sizes shown in Fig. 38-39 are hypothetical and are chosen to demonstrate the size effect.

4.33 Effect of Nanoparticle Volume Fraction Distribution

The Mathematica program allows the user to specify a volume fraction of nanoparticles at the top of the fluid and the volume fraction of nanoparticle at the bottom of the fluid, next to the plate. When the nanoparticle diameter is 10 nm, the Mathematica program tolerates a 1-1.5% difference in volume fraction between the top and bottom for the chose conditions. However, the volume fraction difference could be increased by as much as 10% for a nanoparticle diameter of 0.001 nm. For this analysis, the 10 nm diameter nanoparticle size will be used. Figure 40 shows the results from varying the nanoparticle volume fraction at the bottom, next to the plate, for ethylene glycol/alumina nanofluid. Each of the lines are for nanoparticle volume fractions at the top of the nanofluid. Moving from left to right, the nanoparticle volume fractions at the top of the nanofluid are, 0, 0.005, 0.01, 0.015, 0.02, 0.025, and 0.03. For both Fig. 40-41, it is assumed the nanoparticle volume fraction at the plate is greater than the nanoparticle volume fraction at the surface of the nanofluid.

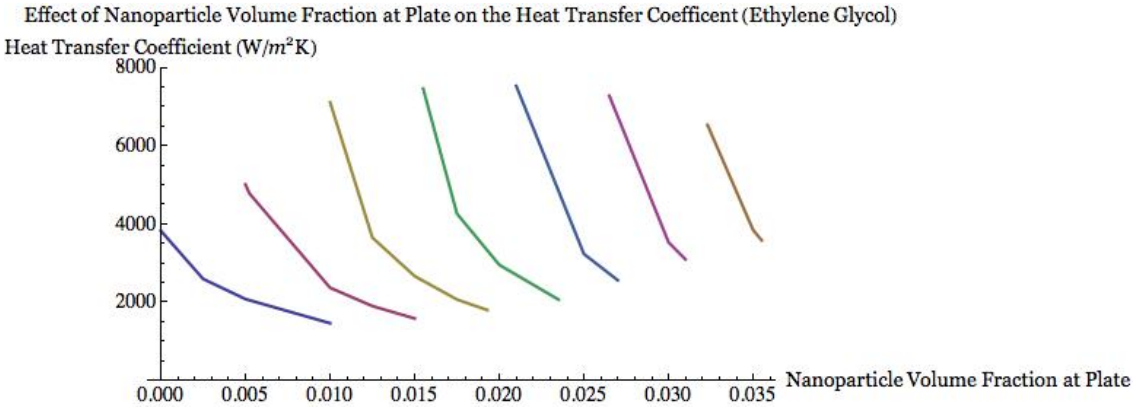

Fig. 40. Variation of nanoparticle distribution on the heat transfer coefficient in alumina/ethylene glycol nanofluid.

As can be seen in the figure above, the heat transfer coefficient increases with increasing volume fraction of nanoparticles. It is also interesting to note that the heat transfer coefficient is largest when the volume fraction at the top of the nanofluid is the same as the volume fraction at the plate. This is because this condition would mean the nanoparticles were evenly dispersed throughout the nanofluid. Figure 41 shows the same information as Fig. 40, and demonstrates the same trends, but it is for water/alumina nanofluid. The lines correspond to top nanoparticle volume fractions of 0.0, 0.01, 0.02, 0.03, 0.04, and 0.05, from left to right, respectively.

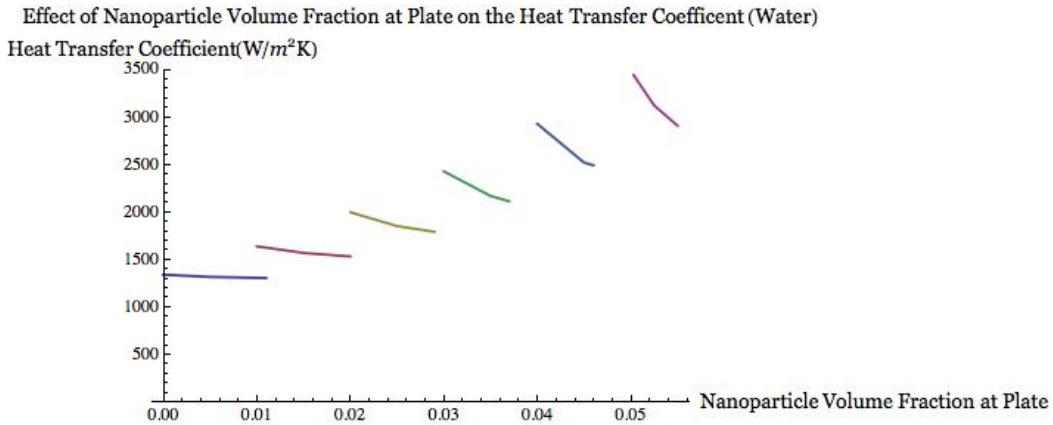

Fig. 41. Variation of nanoparticle distribution on the heat transfer coefficient in alumina/water nanofluid.

By looking at both figures, it is easy to see that the heat transfer coefficient is extremely sensitive to the nanoparticle volume fraction distribution, especially in the case of ethylene glycol nanofluid where the heat transfer coefficient varies from about 2000 to 8000 W/m^2K. The heat transfer coefficient of the water based nanofluid is less sensitive to the nanoparticle volume fraction distribution than the ethylene glycol based nanofluid, but it is still very significant, ranging in heat transfer coefficients of about 1400 to 3500 W/ m^2K. Since both Mathematica programs are the same except for the base fluid properties, it is amazing how the results differ between using different base fluids.

5. CONCLUSION

Nanoparticle diameter size, nanoparticle volume fraction, nanofluid temperature, and free stream velocity have been varied to observe their effects on nanofluid characteristics and the heat transfer coefficient of alumina/water and alumina/ethylene glycol nanofluids under laminar forced convection over a flat plate. Of the parameters studied, the nanoparticle size and volume fraction affected the heat transfer coefficient and flow development the most. Ethylene glycol showed great enhancements due to the addition of nanoparticles compared to water, which correlates with findings from other researchers.

Examining the development of the velocity profile showed that the velocity profile for alumina/ethylene glycol nanofluid became fully developed in a shorter distance along the plate. In addition, increasing the free stream velocity for both types of nanofluid caused the velocity profile to develop a farther distance down the plate.

The nanoparticle volume fraction distribution had a large effect on the heat transfer coefficient. Up to a 1.5% difference between the nanoparticle volume fraction at the bottom of the nanofluid (next to the plate) and the top of the nanofluid was studied. If the nanoparticles are evenly dispersed throughout the fluid, meaning that the nanoparticle volume fraction at the bottom of the nanofluid is the same at the top, the heat transfer coefficient increases by 2 to 3 times compared to having a 1.5% volume fraction difference between the top and bottom. For water, the heat transfer coefficient increased as much as 130% and

for ethylene glycol, the heat transfer coefficient increased by as much as 275%. These results indicate how vital it is for the nanoparticles to stay suspended in the fluid.

As the nanoparticle size was decreased from a nanometer to a picometer, there was a significant increase in the heat transfer coefficient, about a 16% increase in heat transfer coefficient for the water based nanofluid and about a 100% increase for the ethylene glycol based nanofluid. Decreasing the nanoparticle size also dispersed the volume fraction of the nanoparticles farther away from the plate and lowered the temperature next to the plate. Studying the results from sub nano sized particles and noticing the enhancements it had on the heat transfer coefficient indicates that if sub nano sized particles could be produced, the heat transfer capabilities of nanofluids could be improved by using smaller particles.

Many of the heat transfer enhancements were most noticeable when the nanoparticle size became smaller than a nanometer. This is because the nanoparticle volume fraction tended to dip below zero at the nanometer scale in the Mathematica program, but went positive as the nanoparticle diameter became smaller. This issue affected the results, and future work should include some way of prohibiting the nanoparticle volume fraction from going negative. Other improvements to the analysis include adding the effects of agglomeration, fluid nanolayers, transition to turbulence. Backing up results with experimentation is also recommended for the future.

Appendix A

(shown with properties for water)

```
ρp = 3970; cp = 760; ρbf = 977.009; kbf = 613 × 10^(-3); cbf = 4179; μbf = 855 × 10^(-6);
dp = 10 × 10^(-9); kp = 46; kB = 1.38062 × 10^(-23); M = 20; W = 0.1; L = 300; dy = W / (M - 1);

UB = 0; VB = 0; TB = 320; FB = 0.01; UT = 10; VT = 0; TT = 300; FT = 0; Ff = FT; Tf = TT; Uf = UT;

ρ[i_] := ρp ϕ[i][x] + ρbf (1 - ϕ[i][x]); μ[i_] := μbf (1 + 39.11 ϕ[i][x] + 533.9 ϕ[i][x]^2);
k[i_] := kbf (1 + 7.47 ϕ[i][x]); DB[i_] := kB T[i][x] / (3 Pi μ[i] dp);
DT[i_] := (0.26 / (2 + kp / k[i])) (μ[i] / ρ[i]) ϕ[i][x];
DTT[i_] := DT[i] / T[i][x]; c[i_] := ρp cp ϕ[i][x] + ρbf cbf (1 - ϕ[i][x]);

eq[i_] := {u[i]'[x] + (v[i + 1][x] - v[i - 1][x]) / (2 dy) == 0,
   ρ[i] (u[i][x] u[i]'[x] + v[i][x] (u[i + 1][x] - u[i - 1][x]) / (2 dy)) ==
    ((μ[i + 1] + μ[i]) (u[i + 1][x] - u[i][x]) - (μ[i] + μ[i - 1]) (u[i][x] - u[i - 1][x])) / (2 dy^2),
   u[i][x] ϕ[i]'[x] + v[i][x] (ϕ[i + 1][x] - ϕ[i - 1][x]) / (2 dy) ==
    ((DB[i + 1] + DB[i]) (ϕ[i + 1][x] - ϕ[i][x]) - (DB[i] + DB[i - 1]) (ϕ[i][x] - ϕ[i - 1][x])) /
      (2 dy^2) + ((DTT[i + 1] + DTT[i]) (T[i + 1][x] - T[i][x]) -
        (DTT[i] + DTT[i - 1]) (T[i][x] - T[i - 1][x])) / (2 dy^2),
   c[i] (u[i][x] T[i]'[x] + v[i][x] (T[i + 1][x] - T[i - 1][x]) / (2 dy)) ==
    ((k[i + 1] + k[i]) (T[i + 1][x] - T[i][x]) - (k[i] + k[i - 1]) (T[i][x] - T[i - 1][x])) / (2 dy^2) +
     ρp cp (DB[i] (ϕ[i + 1][x] - ϕ[i - 1][x]) (T[i + 1][x] - T[i - 1][x]) / (4 dy^2) +
       DTT[i] (T[i + 1][x] - T[i - 1][x])^2 / (4 dy^2))};

eqB = eq[2] /. {T[1][x] → TB, v[1][x] → VB, u[1][x] → UB, ϕ[1][x] → FB};

eqT = eq[M - 1] /. {T[M][x] → TT, v[M][x] → VT, u[M][x] → UT, ϕ[M][x] → FT};

eqns = Join[Table[eq[i], {i, 3, M - 2}],
   eqT, eqB, Table[u[i][0] == Uf, {i, 2, M - 1}],
   Table[ϕ[i][0] == Ff, {i, 2, M - 1}], Table[T[i][0] == Tf, {i, 2, M - 1}]];

sol = NDSolve[eqns, Flatten[Table[{u[i], v[i], T[i], ϕ[i]}, {i, 2, M - 1}]], {x, 0, L}];

u = Map[Flatten,
   Table[{yj = (j - 1) dy, xi = L (i - 1) / (M - 1), u[j][xi] /. sol}, {j, 2, M - 1}, {i, 1, M - 1}], {2}];

up = ListSurfacePlot3D[u, BoxRatios → {1, 1, 0.5}, Axes → True,
  PlotPoints → 30, AxesLabel → {Style["y", FontFamily → "Arial", FontSize → 14],
    Style["x", FontFamily → "Georgia", FontSize → 14],
    Style["u(x,y)", FontFamily → "Georgia", FontSize → 14]},
  PlotLabel → Style["u Velocity Versus x and y (Oil)", FontFamily → "Georgia", FontSize → 16],
  ViewPoint -> {-2, 2.5, 1.4}]

Plot[Evaluate[Table[u[i][x] /. sol, {i, 2, M - 1, 3}]], {x, 0, L},
 AxesLabel → {Style["x", FontFamily → "Georgia", FontSize → 14],
   Style["u(x,y)", FontFamily → "Georgia", FontSize → 14]},
 PlotRange → All, LabelStyle → (FontFamily → "Georgia"),
 PlotLabel → Style["u Velocity Along Plate Length (Oil)",
   FontFamily → "Georgia", FontSize → 16], AspectRatio → 1 / GoldenRatio]

v = Map[Flatten,
   Table[{yj = (j - 1) dy, xi = L (i - 1) / (M - 1), v[j][xi] /. sol}, {j, 2, M - 1}, {i, 1, M - 1}], {2}];

vp = ListSurfacePlot3D[v, BoxRatios → {1, 1, 0.5},
  Axes → Automatic, PlotPoints → 30, DefaultFont → {"Georgia", 12}, AxesLabel →
   {Style["y", FontFamily → "Georgia", FontSize → 14], Style["x", FontFamily → "Georgia",
     FontSize → 14], Style["v(x,y)", FontFamily → "Georgia", FontSize → 14]},
  PlotLabel → Style["v Velocity Versus x and y (Oil)", FontFamily → "Georgia", FontSize → 16],
  ViewPoint -> {-1.8, 2.5, 1.4}, PlotRange → All]

Plot[Evaluate[Table[v[i][x] /. sol, {i, 2, M - 1, 3}]], {x, 0, L}, PlotRange → All,
 AspectRatio → 1 / GoldenRatio, AxesLabel → {Style["x", FontFamily → "Georgia", FontSize → 14],
   Style["v(x,y)", FontFamily → "Georgia", FontSize → 14]}, PlotLabel →
  Style["y Velocity Along Plate Length (Oil)", FontFamily → "Georgia", FontSize → 16]]

T = Map[Flatten,
   Table[{yj = (j - 1) dy, xi = L (i - 1) / (M - 1), T[j][xi] /. sol}, {j, 2, M - 1}, {i, 1, M - 1}], {2}];
```

```
Tp = ListSurfacePlot3D[T, BoxRatios → {1, 1, 0.5}, Axes → Automatic,
  PlotPoints → 30, AxesLabel → {Style["y", FontFamily → "Georgia", FontSize → 14],
    Style["x", FontFamily → "Georgia", FontSize → 14],
    Style["T(x,y)", FontFamily → "Georgia", FontSize → 14]},
  PlotLabel → Style["Temperature Versus x and y (Oil)", FontFamily → "Georgia", FontSize → 16],
  PlotRange → All, ViewPoint -> {-1.8, 2.5, 1.4}]

Plot[Evaluate[Table[T[i][x] /. sol, {i, 2, M - 1, 3}]], {x, 0, L}, PlotRange → All,
 AspectRatio → 1 / GoldenRatio, AxesLabel → {Style["x", FontFamily → "Georgia", FontSize → 14],
   Style["T(x,y)", FontFamily → "Georgia", FontSize → 14]}, PlotLabel →
  Style["Temperature Along Plate Length (Oil)", FontFamily → "Georgia", FontSize → 14]]

Phi = Map[Flatten,
   Table[{yj = (j - 1) dy, xi = L (i - 1) / (M - 1), ϕ[j][xi] /. sol}, {j, 2, M - 1}, {i, 1, M - 1}], {2}];

Fp = ListSurfacePlot3D[Phi, BoxRatios → {1, 1, 0.5},
  Axes → Automatic, PlotPoints → 30, AxesLabel →
   {Style["y", FontFamily → "Georgia", FontSize → 14], Style["x", FontFamily → "Georgia",
     FontSize → 14], Style["ϕ(x,y)", FontFamily → "Georgia", FontSize → 14]},
  PlotLabel → Style["Nanoparticle Volume Fraction Versus x and y (Oil)",
    FontFamily → "Georgia", FontSize → 16], PlotRange → All, ViewPoint -> {-1.8, 2.5, 1.4}]

Plot[Evaluate[Table[ϕ[i][x] /. sol, {i, 2, M - 1, 3}]], {x, 0, L}, PlotRange → All,
 AspectRatio → 1 / GoldenRatio, AxesLabel → {Style["x", FontFamily → "Georgia", FontSize → 14],
   Style["ϕ(x,y)", FontFamily → "Georgia", FontSize → 14]},
 PlotLabel → Style["Nanoparticle Volume Fraction Along Plate Length (Oil)",
   FontFamily → "Georgia", FontSize → 16]]
```

BIBLIOGRAPHY

1. Yu, W., France, D. M., Routbort, J. L., Choi, S. U. S., 2008. Review and Comparison of Nanofluid Thermal Conductivity and Heat Transfer Enhancements. Heat Transfer Engineering. 29(5), 432-460 (1).
2. Jang, S. P., Choi, S. U. S. 2007. Effects of Various Parameters on Nanofluid Thermal Conductivity. Journal of Heat Transfer. 129, 617-623.
3. Maxwell, J. C., A Treatise on Electricity and Magnetism, third ed., Oxford University Press, London, 1892.
4. Hamilton, R. L., Crosser, O. K., 1962. Thermal Conductivity of Heterogeneous Two-Component Systems. I & EC Fundamentals 1, 187-191.
5. Ren, Y., Xie, H., Cai, A., 2005. Effective Thermal Conductivity of Nanofluids Containing Spherical Nanoparticles. Journal of Physics D: Applied Physics. 38, 3958-3961.
6. Beck, M. P., Sun, T., Teja, A. S., 2007. The Thermal Conductivity of Alumina Nanoparticles Dispersed in Ethylene Glycol. Fluid Phase Equilibria. 260, 275-278.
7. Karthikeyan, N. R., Philip, J., Raj, B., 2008. Effect of Clustering on the Thermal Conductivity of Nanofluids. Materials Chemistry and Physics. 109. 50-55.
8. Prakash, M., Giannelis, E. P., 2007. Mechanism of Heat Transport in Nanofluids. Journal of Computer-Aided Material Design. 14, 109-117.
9. Wang, X., Xu, X., Choi, S. U. S., 1999. Thermal Conducivity of Nanoparticle-Fluid Mixture. Journal fo Thermophysics and Heat Transfer. 13(4), 474-480.
10. Jang, S. P., and Choi, S. U. S., 2004. Role of Brownian Motion in the Enhanced Thermal conductivity of Nanofluids. Applied Physics Letters. 84, 4316-4318.
11. Chon, C. H., Kihm, K. D., Lee, S. P., Choi, S. U. S. 2005. Empirical Correlation Finding the role of Temperature and Particle Size for Nanofluid (Al_2O_3) Thermal Conductivity Enhancement. Applied Physics Letters. 87, 153107.
12. Prasher, R., Bhattacharya, P., Phelan, P. E., 2006. Brownian-Motion-Based Convective-Conductive Model or the Effective Thermal Conductivity of Nanofluids. Journal of Heat Transfer. 128, 588-595.
13. Ki, J., Kang, Y. T., and Choi, C. K., 2004. Analysis of Convective Instability and Heat Transfer Characteristics of Nanofluids. Physics of Fluids, 16 (7), 2395-2401.
14. Evans, W., Fish, J., Keblinski, P., 2006. Role of Brownian Motion Hydrodynamics on Nonofluid Thermal Conductivity. Applied Physics Letters. 88, 093116.
15. Keblinski, P., Eastman, J. A., Cahill, D. G., 2005. Nanofluids for Thermal Transport. Materials Today. June. 36-44.

16. Yu, C. J., Richter, A. G., Datta, A., Durbin, M. K., Dutta, P., 1999, Observation of Molecular Layering in Thin Liquid Films Using X-Ray Reflectivity. Physical Review Letters, 82, 2326-2329.
17. Buongiorno, J. 2006. Convective Transport in Nanofluids. Journal of Heat Transfer, 128, 240-250.
18. Garg, J., Poudel, B., Chiesa, M. et. al. 2008. Enhanced Thermal Conductivity and Viscosity of Copper Nanoparticles in Ethylene Glycol Nanofluid. Journal fo Applied Physics. 103. 074301.
19. Mansour, R. B., Galanis, N., Nguyen, C.T. 2007. Effect of Uncertainties in Physical Properties on Forced Convection Heat Transfer with Nanofluids. Applied Thermal Engineering. 27. 240-249.
20. Zhou, S. Q., Rui, N. 2008. Measurement of the Specific Heat Capacity of Water-based Al_2O_3 Nanofluid. Applied Physics Letters. 92, 093123.
21. Prasher, R., Song, D., Wang, J., Phelan, P. 2006. Measurements of Nanofluid Viscosity and its Implications for Thermal Applications. Applied Physics Letters, 89, 133108.
22. Pak, B. C., Cho, Y. I., 1998. Hydrodynamic and Heat Transfer Study of Dispersed Fluids with Submicron Metallic Oxide Particles. Experimental Heat Transfer. 11(2), 151-170.
23. Behzadmehr, A., Saffar-Avval, M., Galanis, N. 2007. Prediction of Turbulent Forced Convection of a Nanofluid in a Tube with Uniform Heat Flux Using a Two Phase Approach. International Journal of Heat and Fluid Flow. 28, 211-219.
24. Maiga, S. E. B., Palm, S. J., Nguyen, C. T., et. al. 2005. Heat Transfer Enhancement by Using Nanofluids in Forced Convection Flows. International Journal of Heat and Fluid Flow, 26, 530-546.
25. Heris, S. Z., Esfahany, M. N., Etemad, S. G. 2007. Experimental Investigation of Convective Heat Transfer of Al_2O_3/water Nanofluid in Circular Tube. International Journal of Heat and Fluid Flow, 28, 203-210.
26. Xuan, Y., Li, Q., 2003. Investigation on Convective Heat Transfer and Flow Features of Nanofluids. Journal of Heat Transfer. 125(1), 151-155.
27. Nguyen, C. T., Roy, G., Gauthier, C. et al., 2007. Heat Transfer Enhancement Using Al_2O_3-water Nanofluid for an Electronic Liquid Cooling System. Applied Thermal Engineering. 27, 1501-1506.
28. McNab, G. S., Meisen, A., 1973. Thermophoresis in Liquids. Journal of Colloid Interface Science. 44(2), 339.
29. Tzou, D. Y., 2008. Nanofluids. Class notes from MAE 8300, University of Missouri-Columbia
30. Tzou, D. Y., 2006. Computational Techniques for Microscale Heat Transfer, In Minkowyca, W. J., Sparrow, E. M., and Murphy (Eds.), Handbook of Numerical Heat Transfer, 2nd edition (Chap. 20). New York: Wiley.